
Article:
Malone, L.A. orcid.org/0000-0002-7625-7545, Proctor, M.S., Hitchcock, A. et al. (2 more authors) (2021) Cytochrome b6f – orchestrator of photosynthetic electron transfer. Biochimica et Biophysica Acta (BBA) - Bioenergetics, 1862 (5). 148380. ISSN 0005-2728

https://doi.org/10.1016/j.bbabio.2021.148380

Cytochrome b_6f – orchestrator of photosynthetic electron transfer

Lorna A. Malone, Matthew S. Proctor, Andrew Hitchcock, C. Neil Hunter & Matthew P. Johnson*

Department of Molecular Biology and Biotechnology, University of Sheffield, Sheffield S10 2TN, UK.

*Author for correspondence: matt.johnson@sheffield.ac.uk

Highlights

- Cytb_6f couples electron transfer between PSI and PSII to the generation of proton motive force via the Q-cycle.
- Key features of Cytb_6f mitigate the formation of damaging reactive oxygen species and avoid short-circuits of the Q-cycle.
- Cytb_6f catalyses the rate-limiting step in linear electron transfer and is downregulated by ΔpH to protect PSI from damage.
- Cytb_6f may act as the elusive antimycin-A sensitive ferredoxin-quinone reductase involved in cyclic electron transfer.
- Cytb_6f is a redox-sensing hub responsible for triggering photosynthetic acclimation via the STN7/ STT7 kinase.

Keywords: cytochrome b_6f; photosynthesis; Q-cycle; linear electron transfer; cyclic electron transfer; redox regulation; transmembrane signalling.

Abstract

Cytochrome b_6f (cytb_6f) lies at the heart of the light-dependent reactions of oxygenic photosynthesis, where it serves as a link between photosystem II (PSII) and photosystem I (PSI) through the oxidation and reduction of the electron carriers plastoquinol (PQH_2) and plastocyanin (Pc). A mechanism of electron bifurcation, known as the Q-cycle, couples electron transfer to the generation of a transmembrane proton gradient for ATP synthesis. Cytb_6f catalyses the rate-limiting step in linear electron transfer (LET), is pivotal for cyclic electron transfer (CET) and plays a key role as a redox-sensing hub involved in the regulation of light-harvesting, electron transfer and photosynthetic gene expression. Together, these characteristics make cytb_6f a judicious target for genetic manipulation to enhance photosynthetic yield, a strategy which already shows promise. In this review we will outline the structure and function of cytb_6f with a particular focus on new insights provided by the recent high-resolution map of the complex from Spinach.

1. Introduction

The year 2020 marks 45 years since Peter Mitchell proposed the Q-cycle mechanism that underpins our understanding of the cytochrome bc_1 (cytbc_1) and cytochrome b_6f (cytb_6f) complexes [1]. These two Rieske/cytochrome *b* type complexes are part of a larger superfamily that is widely distributed in eukaryotic and prokaryotic photosynthetic and respiratory electron transport chains [2]. In oxygenic phototrophs such as plants, algae and cyanobacteria, cytb_6f not only provides an essential electronic connection between the light-powered chlorophyll-protein complexes, photosystem I and II (PSI and PSII), but also acts as the major coupling site in photosynthesis, transferring four of the six protons moved to the thylakoid lumen per $NADP^+$ molecule reduced by the linear electron transfer (LET) chain [3–8](Fig. 1). Its simultaneous roles in oxidising plastoquinol (PQH_2) and reducing plastoquinone (PQ) via the Q-cycle has led to the suggestion that cytb_6f is also the elusive ferredoxin (Fd)-PQ reductase (FQR) involved in the major pathway of cyclic electron transfer (CET1) [9–12](Fig. 1). Thus, cytb_6f is uniquely suited to sensing the redox state of the electron transfer chain and the chloroplast stroma/cytoplasm, interacting with various regulatory elements that transduce these signals to optimise photosynthesis in fluctuating environmental and metabolic conditions [4,13,14]. In recent years, there have been a number of studies that significantly enhance our understanding of this extraordinary complex, shedding light on the internal mechanics of the Q-cycle and providing new clues as to how it fulfils its various roles in photosynthetic regulation [15–22]. Combining this latest information with the recently reported high-resolution structure of the higher plant cytb_6f [23], we review the current state of knowledge regarding this crucial complex and highlight those areas where our understanding has evolved.

2. Structural overview of the cytb_6f complex

To date, high-resolution structures of cytb_6f are available from four different species; the higher plant *Spinacia oleracea* (Spinach) [23], the green alga *Chlamydomonas reinhardtii* (*Chlamydomonas*) [24], and the filamentous cyanobacteria *Nostoc* sp. PCC 7120 (*Nostoc*) [18,22,25] and *Mastigocladus* (*M.*) *laminosus* [18,26–30]. These structures show that cytb_6f is a ~220 kDa functional dimer with each monomeric unit made up of four major subunits: cytochrome *f* (cyt*f*) (PetA), cytochrome b_6 (cytb_6) (PetB), the Rieske iron-sulphur protein (ISP) (PetC) and subunit IV (subIV) (PetD) as well as four minor subunits (PetG, L, M, N) (Table 1). Cytb_6f displays a strong similarity to the respiratory cytbc_1 complex found in

mitochondria and anoxygenic photosynthetic bacteria [31–33], with significant conservation of the core redox components, which are encased within a central four-helix bundle (Fig. 2). In cytb_6f, this core helical bundle is provided by the cytb_6 subunit (helices A-D) which also binds two *b*-type haems (haems b_n and b_p) and a *c*' (high-spin)-type haem (haem c_n) (Fig 2A,D,G). Surrounding the core of the cytb_6f complex are several additional transmembrane helices (TMHs), including three from subIV (E-G), four from each of the four small subunits (Pet G, L, M, N) and two single TMHs which anchor the p-side extrinsic subunits (cyt*f* and the ISP) (Fig 2G). On the p-side of the complex, both cyt*f* and the ISP protrude into the thylakoid lumen with the long β-sheet rich domain of cyt*f* encompassing the smaller globular domain of the ISP (Fig. 2A). Within these lumenal-facing domains, cyt*f* binds a *c*-type haem (but called haem *f,* from *'frons'* meaning leaf in Latin), while the ISP binds a 2Fe-2S cluster. In cytbc_1, both the core helical bundle (A-D) and the three TMHs (E-G) are provided by the cytochrome *b* subunit, which coordinates haems b_n and b_p, though the additional haem c_n is absent (Fig 2D-I). As in cytb_6f, cytbc_1 binds a 2Fe-2S cluster within its ISP subunit and a *c*-type haem within its peripheral subunit cytochrome c_1 (cytc_1) (Fig 2D-F). It is interesting to note from an evolutionary perspective that cyt*f* and cytc_1 are not related but are rather an example of convergent evolution [2]. Unlike cytbc_1, cytb_6f also contains two additional pigment molecules per monomer, one chlorophyll *a* (Chl *a*) and one 9-cis β-carotene (Fig 2D). These pigments are found associated with subIV but their exact functions remain unclear. PetO [34] and PetP [35] are also present in the *Chlamydomonas* and cyanobacterial cytb_6f complexes, respectively, though to date, they have not been identified in any of the high-resolution structures so far published.

In both cytb_6f and cytbc_1, the overall structure is stabilised through domain swapping of the p-side extrinsic domain of the ISP, forming an interlinked dimeric complex [24,26]. This structure is further stabilised by interactions formed between residues of cytb_6 and subIV as well as several protein-lipid interactions involving lipids of the membrane bilayer [22]. While the identity of these lipids varies between species due to their differing membrane compositions, nine native lipid molecules are resolved in the spinach complex (two monogalactosyldiacylglycerol (MGDG), four phosphatidylglycerol (PG), three sulfoquinovosyldiacylglycerol (SG)) in addition to three phosphatidylcholine (PCH) molecules added during purification [23]. In addition to the essential role of these lipids in stabilising the dimeric structure, it has also been speculated that several of these lipid binding sites may have crucial roles in the functions of the cytb_6f complex [22,30]. Between the two

monomeric units of the complex lies a large protein-free cavity providing a space to sequester an internal pool of PQ/PQH_2 [22–24,26]. On the inside walls of this cavity lie two substrate binding sites, one near the p-side of the complex (Q_p) which serves as the site of PQH_2 oxidation, and one near the n-side (Q_n) which is the site of PQ reduction [23,24,26].

3. The modified Q-cycle and electron transfer mechanics

The Q-cycle, first proposed by Peter Mitchell in 1975 [1] and later modified by Tony Crofts [36,37] suggests that quinol oxidation in cytbc_1 and cytb_6f complexes follows a mechanism of electron bifurcation. The overall process can be split into two half-reactions as depicted in in Fig 3A-B. In cytb_6f, the first half-cycle involves transfer of the two electrons derived from PQH_2 oxidation at the Q_p site into the high-potential (2Fe-2S and haem *f*) and low-potential (haems b_p, b_n and c_n) chains (Fig 3A). In the high-potential chain, the electron is transferred from the $PQ^{\bullet-}$/PQH_2 couple (+480 mV) to the nearby 2Fe-2S cluster of the ISP (+310 mV) (Fig 3C). This in turn facilitates transfer of the electron to haem *f* (+355 mV) to the single-electron acceptor protein Pc (+370 mV) bound on the p-side of the complex and onward to P700, the PSI primary donor (+480 mV)(Fig 3C). In the low-potential chain, the second electron derived from the PQ/ $PQ^{\bullet-}$ couple (-280 mV) reduces nearby haem b_p (-150 mV) and then haem b_n (-85 mV) (Fig 3C). This transfer of electrons across the bilayer between the two *b*-haems is electrogenic, contributing to the electric field component ($\Delta\psi$) of the *pmf* and is responsible for the b-phase of the electrochromic carotenoid band shift (ECS) signal [38,39]. Following the reduction of haem b_n, the electron is then transferred to the nearby haem c_n (+100 mV), which forms part of the Q_n PQ binding site. The two protons liberated by the oxidation of PQH_2 at the Q_p site are transferred to the thylakoid lumen (p-side), contributing to the ΔpH component of the *pmf*. In the second half-cycle (Fig 3B), another PQH_2 molecule is oxidised at the Q_p site, prompting the transfer of a further two protons to the lumen and the reduction of a second Pc molecule via the high potential chain, while the second electron enters the low potential chain, resulting in the production of a haem c_n^{red}/ b_n^{red} pair. Following formation of this highly reducing redox-coupled pair, haem c_n facilitates the quasi-concerted two electron-two proton reduction of PQ to PQH_2 at the Q_n site in a so-called 'double-barrelled shotgun' mechanism (Fig 3B-C) [3,4,40,41].

According to the basic Q-cycle mechanism given above, the first electron from the PQH_2 molecule is transferred to the 2Fe-2S cluster and then on to a haem *f* (cyt*f*). While this transfer is observed to occur on a timescale of 2-5 ms [42], it is evident from existing

structures of cytb_6f that the two cofactors are separated by too large a distance (~26 Å) to allow such rapid ET according to the Moser-Dutton 'ruler' [23,24,26,43]. In the cytbc_1 complex, this apparent juxtaposition between the observed and theoretical ET rates is readily explained by a large-scale conformational change in the extrinsic domain of the ISP [33](Fig 4) (Supplementary Video 1). This conformational change, observed in the high-resolution structures of the chicken (*Gallus gallus*) cytbc_1 complex (PDB IDs: 3BCC; 1BCC), brings the 2Fe-2S cluster from a Q_p proximal position (~27 Å away from haem c_1) to a position ~16 Å from the *c*-type haem acceptor (Q_p distal) (Table 2). In this manner, the cytbc_1 complex is able to bridge the large distance between the Q_p site and the *c*-type haem acceptor of the cytc_1 subunit enabling electron transfer down the high-potential chain to the soluble cytc/c_2 electron acceptor. While it is hypothesised that a similar mechanism must exist in cytb_6f [3,14], so far, no direct structural evidence exists to support this. Moreover, mutations in the proline-rich hinge region between the lumenal and TM domains of the ISP have been shown to have little effect on cytb_6f activity despite analogous changes in cytbc_1 proving detrimental to catalytic turnover [44,45]. Despite the lack of a high-resolution structure of the putative Q_p distal conformation for cytb_6f, a range of experimental data support the existence of such a conformational transition [46–49]. It therefore remains likely that a conformational change occurs on the p-side of the complex to mitigate the distance between the 2Fe-2S cluster and haem *f* but that such a change may be i) limited by crystal contacts in many of the cytb_6f structures containing quinone analogue inhibitors, ii) occurring in a different manner, such as through movement of the peripheral *c*-type haem containing cyt*f* subunit rather than through the ISP[50]. Further work is required to distinguish between these possibilities.

4. Architecture and dynamics of the Q_p site

In both cytb_6f and cytbc_1, the Q_p site is located at the end of a long, narrow hydrophobic portal located on the inner wall of the intermonomer cavity near the p-side of the complex [23,24,26,29,31–33]. While the architecture of this portal is mostly conserved in both complexes (Fig 5A-F), the portal is significantly narrowed in cytb_6f by the presence of a Chl *a* molecule (Fig 5B, G). In the spinach structure, the chlorin head group of the Chl *a* is observed between the F and G helices of subIV while the long phytyl tail of the molecule protrudes into the Q_p portal [23](Fig 5D, G). It is interesting to note that two conformations of the phytyl tail are also resolved in this study: the first appears to permit access to the Q_p site ('open' conformation) while the second appears to restrict access ('closed' conformation)

(Fig 5H). Movement of the phytyl tail between these two conformations, together with some slight movement of surrounding residues, appears to contribute to further narrowing of the Q_p portal as depicted in Fig 5H (Supplementary Video 2). While native quinol binding has not been structurally resolved within the Q_p site of either cytbc_1 or cytb_6f to date, substrate binding in both complexes has been probed using quinol analogue inhibitors such as stigmatellin (STG, cytbc_1), myxothiazol (MYX, cytbc_1) and tridecylstigmatellin (TDS, cytb_6f) [18] (Fig 5E,F).

In cytbc_1, the Q_p site forms a bifurcated volume with one lobe forking towards the 2Fe-2S cluster while the other extends towards haem b_p (Fig 6A-C). It is apparent from quinone analogue studies that these two lobes are preferred by different classes of analogue inhibitor, with the 2Fe-2S and haem b_p proximal lobes preferred by inhibitors that mimic ubiquinone (UQ) (e.g. stigmatellin and 5-*n*-undecyl-6-hydroxy-4,7-dioxobenzothiaole) and semiubiquinone (UQH) (e.g. myxothiazole and β-methoxyacrylatestilbene (MOAS)-type inhibitors) species respectively [51,52]. Since occupation of either lobe is a mutually exclusive event, these observations indicate that the quinone species may undergo movement within the Q_p site during catalysis [51]. It is thought that binding initially occurs within the 2Fe-2S proximal lobe where the first oxidation and deprotonation event is facilitated by the 2Fe-2S cluster together with one of its coordinating Histidine residues (His161, *G. gallus* numbering) (Fig 6A). Subsequent movement of the UQH species within the bifurcated volume facilitates a second deprotonation event via the highly conserved Glu272 residue (PEWY motif) at the base of the second lobe (Fig 6B); this in turn allows an electron to be transferred from $UQ^{\bullet-}$ to haem b_p. The subsequent attraction between protonated Glu272 and reduced haem b_p induces a conformational change in the side chain of Glu272 away from the Q_p site allowing proton exit to the aqueous p-side (this alternate conformation of Glu272 is observed in the MYX inhibited cytbc_1 structure, Fig 6C). As in cytbc_1, the Q_p site in cytb_6f appears to be forked, with the His128 residue coordinating the 2Fe-2S ISP cluster at the end of one branch and a Glu78 residue and haem b_p at the end of the other (Fig 6D). Similarly, deprotonation of PQH_2 is likely carried out by the analogous residues in cytb_6f, His128 and Glu78 (spinach numbering) [4,18,53](Fig 6D).

The first deprotonation of PQH_2 to form the species PQH^- and its subsequent oxidation by the 2Fe-2S cluster to form PQH represent the rate-limiting steps in cytb_6f turnover [4,50]. These forward endergonic reactions (with small forward rate constants) (Fig 3C) are made possible by their close coupling with the second exergonic

deprotonation/oxidation steps (with large forward rate constants) involving Glu78 and haem b_p that generate PQ (Fig 3C). The redox potential of the PQ/$PQ^{\bullet-}$ couple is ~-280mV, sufficient to reduce haem b_p (-150 mV) of the low potential chain [4,5]. In cytbc_1 the conformational change in Glu272 causes the rotation of the side chain away from the substrate in the Q_p site and may facilitate its release (Fig 6C) [54,55]. Although such a movement of the PEWY Glu78 has not been observed in cytb_6f, it is postulated that a similar mechanism would occur [18,50]. Temporary absence of the Q_p site during the reaction cycle in cytb_6f and cytbc_1 complexes was suggested to be mitigated by a 'stand-by' site for quinol binding that would facilitate its rapid provision upon return of the ISP and Glu78 to their original positions [6]. Indeed, in the recent spinach cytb_6f structure, a well-defined PQH_2 molecule was resolved in a position adjacent to the Chl *a* tail approaching the entrance to the Q_p portal [23](Fig 5G). Interestingly, mutation of Glu78 in *Chlamydomonas* to Lys or Leu significantly slowed but did not abolish PQH_2 oxidation, while mutation to Gln or Asn increased the electrogenicity of the complex [53]. This is consistent with the fact that Glu78 sits at the mouth of a hydrophilic tunnel that has been proposed as being an exit route for the second proton from the Q_p site (Fig 6E) [18,53,56]. This proposal is further supported by evidence from the spinach cytb_6f structure, whereby the highly conserved Glu78 is observed in a haem b_p proximal position facing away from the Q_p site and towards a channel lined by a number of conserved hydrophilic residues including Arg87 (cytb_6), Ser91 (cytb_6), Glu3 (PetG), Glu58 (subIV), Lys145 (cyt*f*), Glu242 (cyt*f*), Glu5 (PetM) and Glu34 (cyt*f*) [23]. Although the spinach structure is limited by resolution, it is expected that this p-side exposed channel would be highly hydrated as detailed in the original proposal for the *Nostoc* cytb_6f [18] (Fig 6E).

5. Architecture and dynamics of the Q_n site

A major difference between the cytb_6f and cytbc_1 complexes is the structure of Q_n site (Fig 7A-D). Although the position of haem b_n is highly conserved between cytbc_1 and cytb_6f [7], the space between haem b_n and the intermonomer cavity in cytb_6f is further occupied by a penta-coordinated *c'*-type (high-spin) haem (c_n) covalently bound by a single thioether linkage to Cys35 of cytb_6 [22–24,26–28,40,57,58] (Fig 7B, D). It is located approximately 4 Å away from haem b_n with a water molecule/hydroxide ion intervening between the two macrocycle rings and acting as a putative axial ligand to c_n. In this position, haem c_n occupies a location approximately equivalent to the UQ binding site (Q_n) in cytbc_1, with its open axial

position facing outwards towards the quinone exchange cavity (Fig 7E-H). Despite the conservation of function elsewhere between cytbc_1 and cytb_6f, the presence of the additional haem c_n and apparent obstruction of the putative Q_n site suggests that the quinone reduction mechanism in cytb_6f differs significantly from that of cytbc_1 [7,40,57,59]. While in cytbc_1, UQ reduction is facilitated by a two-step electron transfer from haem b_n resulting in a UQ•- intermediate [60], no such intermediate has been detected in cytb_6f. Additionally, while in cytbc_1 these n-side reduction reactions are specifically inhibited by antimycin A [61,62], this effect is absent in cytb_6f [63].

Given these observations, an alternative reduction mechanism likely exists in cytb_6f which incorporates haem c_n [7,40,57,59]. In this mechanism, the second electron derived from PQH_2 oxidation may be transferred along the low potential chain through haem b_p (-150 mV) to haem b_n (-85 mV), and then onto haem c_n (+100 mV) (Fig 3C). However, this situation is further complicated by several additional factors: i) the redox equilibrium between haems b_n and c_n is sensitive to the $\Delta\psi$ [64], with a larger field favouring the b_n^{red}/c_n^{ox} pair; ii) the redox titration of the haem c_n in the *Chlamydomonas* complex shows a marked pH dependence (-60 mV/pH unit) varying from +175 mV at pH 6 to -50 mV at pH 9 [40,59]; and iii) the midpoint potential of haem c_n is further shifted to -150 mV at pH 7 in the presence of the Q_n site inhibitor and semiquinone analogue 2-n-nonyl-4-hydroxyquinoline N-oxide (NQNO) [40]. This last point is explained by the observation that NQNO (and indeed TDS) acts as an axial ligand to haem c_n [28] (Fig 7E, F). A similar downshift in midpoint potential is also observed in a Phe40Tyr (subIV) mutant in *Chlamydomonas*, suggesting that the additional hydroxyl group of Tyr provides an axial ligand to the haem c_n [59]. While these findings demonstrate that the local environment strongly influences the redox properties of haem c_n and suggest that it facilitates the binding of PQ [40], EPR evidence indicates that haem c_n remains penta-coordinated [57]. This apparent discrepancy is clarified by the most recent structure of cytb_6f from spinach [23], where a native PQ molecule is observed bound to the Q_n site (Fig 7H). Unlike NQNO (Fig 7E), the native PQ molecule does not act as an axial ligand, instead forming a close association with one of the haem c_n propionates (Fig 7G). Moreover, while the semiubiquinone intermediate at the Q_n site in cytbc_1 is stabilised by multiple interactions from surrounding residues (His202, Asp229, K228 and Ser206; *G. gallus* cytbc_1 numbering) and water molecules [33,65,66](Fig 7H), the substrate in spinach cytb_6f is apparently only stabilised by a single interaction with the haem c_n propionate (Fig 7G).

Interestingly, while PQ is observed bound to the Q_n site on one side of the dimeric spinach structure, the other site remains empty [23]. Comparison of the unoccupied (Fig 8A) and occupied (Fig 8B) halves of the dimer reveal several conformational changes in both the haem c_n propionate group and nearby residues (Arg207 and Asp20; cytb_6) which may underlie PQ binding and reduction at the Q_n site (Supplementary Video 3). While in the unoccupied Q_n-site, a H-bonding network appears to be formed between the haem c_n propionate, Arg207 and Asp20 (Fig 8A), this network is disturbed in the opposing monomer by the binding of PQ (Fig 8B). In particular, the binding of PQ appears be accommodated by a rotation of the haem c_n propionate away from Arg207 and towards the 1,4-benzoquinone head group of the incoming PQ molecule (Fig 8B). These observations, together with the evidence that reduction of haem c_n is coupled to its protonation [40,57], suggest a plausible scenario for PQ binding involving the reduction of haem c_n by haem b_n and protonation of the haem c_n propionate by nearby Arg207. Rotation of the haem c_n propionate group upon its protonation would break the interaction with Arg207 allowing it to act as an H-bond donor to the carbonyl oxygen on the 1,4-benzoquinone ring of PQ [23](Fig 8B). This mode of binding would stabilise the quinone, rather than the semiquinone as in cytbc_1, leaving the redox potential of the $PQ/PQ^{\bullet-}$ couple at ~-280 mV (as in solution). In this scenario, the first endergonic reduction of PQ by haem c_n would only become likely when a second electron was also available in the low potential chain to allow the subsequent exergonic reduction of the $PQ^{\bullet-}/PQH_2$ couple (+480 mV). In this manner, the presence of haem c_n may ensure that the $PQ^{\bullet-}$ species has a very low equilibrium population and that electron transfer can only proceed via a quasi-concerted 'double-barrelled shotgun' mechanism when the b_n^{red}/c_n^{red} pair is present [40,41,59].

The reduction of PQ would subsequently allow its protonation with the first proton provided via the haem c_n propionate upon its oxidation. Protonation events at the Q_n site are promoted by $\Delta\psi$, which causes the stromal side of the membrane to become more negatively charged thus attracting protons [9,67], while high ΔpH, which increases the stromal pH acts antagonistically [9,39]. Provision of a second proton to the Q_n site from the stroma may involve the highly conserved Glu29 and Asp35 residues (the E/D pathway) of cytb_6f [18] (Fig 8C-D). As the side-chain oxygen of Asp35 is too far away from the 1,4-benzoquinone ring oxygen for hydrogen-bond formation (~8.9 Å) in the spinach structure, it is possible that an ordered water molecule acts as a bridge to link the E/D pathway to the bound PQ molecule (Fig 8E-F). The existence of such a proton channel at the Q_n site was predicted by the

inhibitory action of triorganitins on haem b_n/b_p oxidation and the electrogenic reaction [68]. In the spinach structure, there are some regions of unassigned density between Asp35 and the PQ molecule which are consistent with bridging water molecules, however a higher resolution structure would be required to confirm this hypothesis.

Another salient feature of the Q_n site revealed in the spinach cytb_6f structure, is the bowed conformation adopted by the bound PQ molecule with the isoprenoid tail straddling the intermonomer cavity and thereby partially obstructing the Q_n site on the neighbouring monomer (Fig 9A-C) [23]. It is interesting to note that this orientation of the PQ molecule may prevent simultaneous binding of PQ at both Q_n sites within the dimer (Fig. 9B). In this instance, any electron entering the low potential chain on the monomer bearing an empty Q_n site could be transferred rapidly to the neighbouring monomer via the 15.3 Å electron-tunnelling distance between the b_p haems (Fig 9C) [69]. Such tunnelling would be rendered more likely if the reduced, protonated form of haem c_n were to be stabilised by PQ as suggested above, since the enhanced potential difference between the two low potential chains would provide a driving force for electron tunnelling (Fig 9D). This suggestion could explain the observation that the haem c_n midpoint potential shows heterogeneity that is abolished upon addition of NQNO[40,57]. Since NQNO has a shorter tail than the native PQ, its binding may not prevent binding of a second NQNO at the neighbouring Q_n site. If cytb_6f can operate according to this 'electronic bus-bar' principal [69], this mechanism could provide a means to avoid competition between the two Q_n sites for electrons, favouring a more rapid turnover of the low potential chain and thus increasing the efficiency of the Q-cycle.

In addition to providing insights into the mechanics at the Q_n site, the spinach cytb_6f structure also reveals interesting insights into the movements of PQ/PQH_2 within the intermonomer cavity. While it has previously been suggested that substrate could exchange between the Q_p and Q_n sites within the intermonomer cavity [11,70], until now there has been no direct structural evidence to support such a suggestion. In the recent spinach cytb_6f structure, an additional PQ molecule is observed traversing between the Q_p and Q_n sites in opposing monomeric units providing direct evidence for 'diagonal' PQ/PQH_2 exchange within the intermonomer cavity, between opposing halves of the complex. An 'internal' cycle for quinone/quinols within the cytb_6f dimer effectively uncouples turnover at the Q_p and Q_n sites from the larger external PQ pool. Thus, rapid internal exchange of PQ/PQH_2 between

these sites could facilitate more rapid turnover of the Q-cycle, particularly when the external pool is largely reduced.

6. Avoiding short-circuits of the Q-cycle and mitigating superoxide production

In both cytbc_1 and cytb_6f, the reactive oxygen species (ROS) superoxide (O_2^-) can form as a by-product of the Q-cycle due to the transient production of a semiquinone species with sufficient reducing power (-280 mV, $PQ^{\bullet-}/PQH_2$) to reduce the O_2/O_2^- couple (-160 mV) [71,72]. This is particularly problematic for oxygenic phototrophs given that the O_2 concentration is an order of magnitude higher in chloroplasts (where O_2 is a by-product of water oxidation) than in mitochondria (where O_2 is consumed during respiratory electron transfer). Indeed, the rate of superoxide production by cytb_6f is nearly 100 times higher than in cytbc_1 [73]. Another hazard to both cytb_6f and cytbc_1 complexes is the potential for short-circuiting of electrons between the low and high potential chains of the complex, which would undermine *pmf* generation through bypass of the Q-cycle [8,72]. How such short-circuits are avoided and how the production of ROS is largely mitigated has been the subject of intense debate in both cytb_6f and cytbc_1 fields for many years with a variety of models proposed [4–6,8,72].

Given the reversible nature of the PQH_2 oxidation reaction at the Q_p site, it was suggested that binding of substrate and subsequent oxidation reactions may be subject to redox-gating [72]. In this model, PQH_2 will only bind when the redox environment is favourable (i.e. 2Fe-2S^{ox}/b_p^{ox}) and both H-bond acceptors (His128, Glu78) are available. Conversely, in the reverse reaction, PQ may only bind when the redox environment favours this interaction (i.e. 2Fe-2S^{red}/b_p^{red}) and the two catalytically essential residues (His128, Glu78) are available as H-bond donors. In this model, short-circuits may be avoided since the two intermediate redox states which may lead to short-circuit reactions (2Fe-2S^{red}/b_p^{ox} and 2Fe-2S^{ox}/b_p^{red}) are unable to readily bind incoming substrates [5,6,72]. The thermodynamic instability of these states may also explain the failure to crystallise the cytbc_1 or cytb_6f structures with native substrate bound at the Q_p site. Despite the apparent elegance of this mechanism, recent evidence provided by a mutagenesis study using *Chlamydomonas* cytb_6f, aimed at disrupting the Q-cycle, argue against such a strict redox-gating mechanism [19]. In this study, mutants lacking both haems b_n and c_n (His202Gln, cyt b_6) were able to grow photosynthetically despite an apparently 'broken Q-cycle'. Surprisingly, PQH_2 oxidation at the Q_p site and, therefore, cytb_6f turnover remained possible owing to a 'ping-pong' electron

recycling mechanism, albeit with a reduction in the H^+/e^- coupling ratio from 2 to 1. In this scheme, the first turnover of PQH_2 at the Q_p site results in reduction of the 2Fe-2S cluster and haem b_p. This is followed by binding of a second PQH_2 molecule at the Q_p site, irrespective of the presence of the reduced haem b_p. The subsequent oxidation of this second PQH_2 molecule at the Q_p site by the 2Fe-2S cluster is followed by the re-reduction of the $PQ^{\bullet-}$ intermediate by haem b_p, resulting in the regeneration of PQH_2. Crucially, although the endergonic first step in PQH_2 oxidation at the Q_p site transfer via the high potential chain was still driven by these exergonic 'ping-pong' reactions, the subsequent reduction of haem *f* by the 2Fe-2S cluster was much slower in the mutant than the WT, suggesting the reverse reaction of $PQ^{\bullet-}$ reduction by haem b_p is kinetically limited [19].

For many years, detection of the semiquinone at the Q_p site proved elusive, a fact consistent with the suggestion that cytb_6f and cytbc_1 actively destabilise this intermediate, i.e. working contrary to the Pauling principle [8,74]. While destabilisation of the semiquinone would reduce the probability of superoxide production by lowering its steady state population, recent electron paramagnetic resonance spectroscopy (EPR) evidence suggests that these complexes may instead stabilise semiquinone species [15]. The detection of the $PQ^{\bullet-}$ radical at the Q_p site in cytb_6f by EPR suggests that $PQ^{\bullet-}$ at the Q_p site may be stabilised through formation of a spin-coupled state with the reduced 2Fe-2S ISP cluster [15]; this is consistent with an earlier suggestion by Berry and Huang [75]. Stabilisation would increase the midpoint potential of the $PQ/PQ^{\bullet-}$ couple such that reduction of the O_2/O_2^- couple becomes unfavourable. Crucially, the spin-coupled state was observed in the presence of haem b_p/b_n reduction, suggesting it acts as safety feature of the complex when the low potential chain turnover is slowed (e.g. by reduced availability of PQ at the Q_n site) [15]. The existence of the spin-coupled state thereby provides an elegant mechanism that ensures the ISP remains in the Q_p distal position until the second electron derived from Q_p is committed to the low potential chain, simultaneously mitigating ROS formation and avoiding Q-cycle bypass. Once the electron is transferred from $PQ^{\bullet-}$ to haem b_p, the loss of the spin-coupled state allows the ISP to move to the cyt*f* proximal position; this in turn is suggested to change the conformation of the Q_p site enabling the release of PQ.

Further means to avoid ROS production and prevent Q-cycle bypass may be provided by the enigmatic Chl *a* molecule positioned at the entrance to the Q_p site in cytb_6f [76,77] (Fig 5G-H). While it was initially thought that this Chl *a* may actively produce singlet oxygen through triplet energy transfer, it is observed that the excited state lifetime of this Chl

399 *a* molecule is extremely short (~200 ps) compared to other Chl binding proteins (e.g. ~2-4 ns
400 in LHCII) making the triplet energy transfer to O_2 in the cytb_6f complex very unlikely [78–
401 80]. Since β-carotene is also observed at a 1:1 ratio with Chl *a* in cytb_6f, it was initially
402 suggested that this molecule is responsible for the observed quenching [79,80]however, the
403 β-carotene molecule appears to be too far away (19 Å edge-to-edge) from the Chl *a* to allow
404 efficient quenching via the Dexter electron transfer, though quenching via energy transfer
405 may be possible [24,26]. The macrocycle ring of the Chl *a* is located between the F and G
406 helices of subIV, a position occupied by an additional helix in cytbc_1; this, combined with the
407 fact that the dimeric structure of cytb_6f is destabilised upon loss of the Chl *a* molecule,
408 suggest it plays the role of a structural bridge [81]. The Gly136Phe and Val104Phe mutations
409 in the Chl *a* binding site of the *Chlamydomonas* complex stabilised the dimer, but still
410 resulted in a dramatic slowdown in haem *f* reduction, suggesting the Chl *a* plays a crucial role
411 in the activity of the complex [81]. The protrusion of the phytyl tail of Chl *a* towards the
412 mouth of the Q_p binding pocket led to the suggestion that it may gate the Q_p site [82] (Fig
413 5G-H) (See Supplementary Video 2). While the rate of PQH_2 passage to the Q_p site does not
414 appear to be significantly hindered in comparison to cytbc_1, it has been demonstrated using
415 molecular dynamics that the Chl *a* molecule may play a role in retaining substrate within the
416 Q_p site [29]. Given these observations, it is possible that the function of Chl *a* is to prevent
417 semiquinone species from escaping the Q_p site and disproportionating to form PQ and PQH_2.
418 It may therefore work in harmony with the spin-coupling mechanism, outlined above, to
419 prevent Q-cycle bypass. Further roles for Chl *a* in the detection and signalling of redox state
420 are also considered in Section 10.
421
422 **7. Interactions between Pc and cytb_6f.**
423
424 As mentioned in Section 3, the electron acceptor for the high potential chain electron is the
425 soluble protein Pc, though in certain cyanobacteria cytochrome c_6 is present in addition to or
426 in place of Pc [83]. The redox active cofactor in Pc is a copper atom, which cycles between
427 +1/+2 oxidation states [84] as it shuttles between haem *f* and the P700 special-pair Chls of
428 PSI [85]. Such small, water-soluble electron-carrier proteins play a ubiquitous role in both
429 respiratory and photosynthetic electron transfer chains by carrying electrons between integral
430 membrane complexes [86]. To achieve efficient electron shuttling, the interactions between
431 soluble redox proteins and their membrane integral partners must satisfy conflicting
432 requirements they must be: i) highly specific to facilitate efficient electron transfer and ii)

433 sufficiently weak to allow rapid separation following electron transfer in order to sustain high
434 turnover rates. To accomplish this feat, the forces that bring the membrane complex and its
435 soluble partner together must be subsequently reversed following electron transfer to ensure
436 their rapid dissociation. Exactly how these transient electron transfer complexes are
437 reversibly formed within these parameters remains poorly understood [87]. Most current
438 models suggest that soluble redox proteins and their membrane integral partners associate in
439 a stepwise manner, with the first step involving an initial encounter complex steered by long-
440 range electrostatic interactions [87]. The encounter complex is generally thought to be the
441 prelude to the formation of the productive or active electron transfer complex in which short-
442 range hydrophobic interactions between aromatic and non-polar residues surrounding the
443 redox cofactor binding sites are important. The effect of the encounter complex is to bring the
444 electron transfer partners together in an orientated state that minimises the degree of
445 rotational and translational movement of the partners required to find the optimum
446 conformation for productive ET [86,87].
447 The factors that influence both interactions and electron transfer between Pc and
448 cytb_6f have been explored through a variety of studies. In particular, a number of structural
449 and mutational studies indicate the importance of complementary electrostatic interactions
450 between an acidic patch of residues on Pc and a basic patch of residues on cyt*f*, as well as
451 hydrophobic patches surrounding the cofactors of each protein (Fig 10A) [88–94].
452 Interestingly, the positive patches on Pc and negative patches on cyt*f* in the cyanobacterium
453 *Nostoc* indicate reversed electrostatic complementarity [95,96]. The importance of the
454 encounter complex for electron transfer rates is readily demonstrated by their dependence on
455 the ionic strength of the aqueous medium [88,97,98]. At high ionic strength the electron
456 transfer rate declines since the attractive electrostatic interactions are screened. Nuclear
457 magnetic resonance (NMR) studies of biological electron transfer complexes show that the
458 encounter complexes are characterised by very small chemical shift perturbations spread out
459 over relatively large areas of the proteins[93,98]. The interactions that establish ET
460 complexes are therefore highly dynamic, lacking a single well-defined organisation, with any
461 electrostatic interactions and salt-bridges mediated by intervening water molecules [87,99].
462 Recently, new insights into the interaction between Pc and cytb_6f have been provided
463 by single-molecule force spectroscopy (SMFS) employing an atomic force microscope
464 (AFM) (Fig 10B) [20,21]. In these experiments, an AFM probe functionalised with Pc
465 molecules attached via a flexible 10 nm linker is raster scanned across a thylakoid membrane
466 or silicon surface bearing cytb_6f. As the AFM probe bound Pc comes into contact with the

surface it can bind to cytb_6f via translational and rotational movements. The surface dwell-time for the close encounter of the probe and sample at the bottom of the ramp cycle can be lowered to just 50 μs, allowing access to the bound state of the electron transfer complex, which has a lifetime in the range of ~70-400 μs range [85]. The SMFS experiments allow the measurement of the interaction frequency, a relative measurement of the formation of the Pc-cytb_6f complex that is indicative of the association rate of the complex and the unbinding force required to disrupt the cytb_6f-Pc interaction. Using this approach, it was observed that the interaction frequency was significantly reduced as the ionic strength increased, supporting a prominent role for electrostatic interactions in forming the encounter complex [20]. While this indicates a prominent role for electrostatic interactions in the formation of the encounter complex *in vitro*, the role of electrostatic interactions *in vivo* may be less important since the physiologically relevant range of ionic concentrations in the thylakoid lumen is significantly higher (~ 100-350 mM) [100,101]. This conclusion is further corroborated by evidence from site-directed mutagenesis studies in which residues comprising the putative Pc binding site in *Chlamydomonas* (Arg209 and Lys187, 58, 65, and 66), were mutated to Glu. While *in vitro* mutagenesis studies of these residues had a profound effect on cyt*f* oxidation, the impact of these mutations *in vivo* was fairly limited [102,103]. Interestingly, although increased ionic strength in the SMFS experiments had a significant effect on the binding frequency, the unbinding force remained unchanged, suggesting that the Pc-cytb_6f complex is largely mediated by via hydrophobic interactions around the redox cofactors [20].

Further insights gleaned from the SMFS technique include the redox dependency of the Pc-cytb_6f interaction. While prior bulk-phase methods showed no clear redox dependency for these interactions [92], SMFS experiments indicate an element of redox selectivity in the formation of the cytb_6f-Pc complex, both for thylakoid bound cytb_6f and silicon-associated cytb_6f [20,21]. In accordance with these observations, high interaction frequencies are observed for both the cytb_6f^{red}-Pc^{ox} and cytb_6f^{ox}-Pc^{red} pairs; this is consistent with the small thermodynamic driving force (~15-40 mV) and reversibility of the reaction [86]. Additionally, while the interaction frequency between complementary redox partners is notably high, the interaction frequency for the matching redox pairs (cytb_6f^{red}-Pc^{red} and cytb_6f^{ox}-Pc^{ox}) was substantially less (~80-90%) [20,21]. These results indicate that formation of the docking interface is redox-gated (as was also observed in MD simulations of the analogous cytbc_1-cytc_2 interaction [104]) and that, while formation of the electron transfer complex is likely mediated by complementary electrostatic forces, these interactions are significantly aided by the relative charges of the cyt*f* and Pc cofactors. Interestingly, while

the frequency of interaction shows a clear redox-dependency in SMFS experiments, the relative unbinding forces required to disrupt the cytb_6f-Pc complex remain unaffected by the redox states of participants. This observation suggests that once the redox-gated docking interface is established and the cytb_6f-Pc complex is formed (likely through short-range hydrophobic contacts), the same level of force is required to disrupt the cytb_6f-Pc complex regardless of redox states of the two interacting partners. Continued turnover of the cytb_6f complex will regenerate haem f^{red} and produce a strongly disfavoured cytb_6f^{red}-Pc^{red} pair. Therefore, once the two proteins have dissociated, the arrival of another electron on haem *f* will significantly lower the probability of cytb_6f rebinding the just-reduced Pc molecule. Nature likely uses this phenomenon to avoid 'product inhibition', (i.e. unproductive encounters between Pc and cytb_6f molecules in the same redox state), ensuring the efficiency and directionality of the electron transport process [20].

8. The rate-limiting step in linear electron transfer

A key regulatory feature common to both respiratory and photosynthetic electron transfer chains is the feedback control of electron transfer by the ΔpH (known as 'photosynthetic control' in photoautotrophs) [105–107]. The classical view of photosynthetic control is that under permissive low light conditions (Fig. 11A), where LET and (therefore) ΔpH are low, the lumenal pH remains above pH 6.2 [108]. This is crucial since the pKa of the His-ligated ISP 2Fe-2S cluster of cytb_6f varies from ~ pH 8.0 (when reduced) to ~ pH 6.2 (when oxidised)[4]. Therefore, only when the 2Fe-2S cluster is reduced can the ISP His128 ligand (spinach numbering) be protonated, a feature that enables it to act as a H-bond acceptor to the hydroxyl group on the 1,4 benzoquinone ring of PQH_2 (Fig 11B) (see Section 4). Under excess light conditions the rate of LET exceeds their consumption in the downstream metabolism leading to an accumulation of excess electrons at the acceptor-side of PSI (Fig 11C). Over-reduction of PSI promotes the reduction of oxygen to superoxide, which in turn can cause photo-oxidative damage, leading to PSI photoinhibition [109,110]. Since PSI does not possess a rapid repair cycle (unlike PSII), photoinhibition of PSI can have a significant impact on an organism's growth and fitness [111–113]. In phototrophic organisms, these detrimental effects are largely mitigated through photosynthetic control, which serves to limit the build-up of excess electrons on the PSI acceptor-side by controlling the rate of electron donation to the primary PSI electron donor $P700^+$. Photosynthetic control is activated in excess light by the build-up of the ΔpH due to increased CET [114] and/ or the decreased

proton conductivity of the ATP synthase [115]. Increased ΔpH lowers the lumenal pH below pH 6.2, allowing protonation of His128 (Fig 11D). This slows the rate of PQH_2 oxidation at the Q_p site and therefore moderates electron transfer towards P700 (Fig 11E). This mechanism of photosynthetic control is further corroborated by mutagenesis studies in *Arabidopsis* in which the process is manipulated by shifting the pKa of the 2Fe-2S cluster upwards by one pH unit by mutation of Pro143 (ISP) to Leu (Fig 11F). The increase in pKa meant that photosynthetic control is induced in this mutant even under low light conditions, leading to a decrease in the maximal rate of LET [116,117]. A further effect of declining lumenal pH in high light is on the redox potential of the PQH_2/PQ couple, which increases by 59 mV/ pH unit. This reduces the thermodynamic driving force for the high potential chain reactions, which would again act to slow electron transfer [43]. However, should ΔpH remain below ~2 units the large driving force of the PQH_2 to Pc electron transfer (~380 mV) makes a simple mass-action effect on cytb_6f by lumenal pH unlikely [118]. Finazzi et al., [13] instead propose two alternatives to explain the effect of ΔpH on photosynthetic control: i) the protonation of the His128 residue could exert a kinetic effect on cytb_6f by regulating the rate of switching between the distal and proximal positions of the ISP [13] and ii) cytb_6f is regulated by the redox state of the stromal NADPH pool in a pH-dependent fashion [119,120]. Interestingly, *Arabidopsis* plants lacking the stroma-located extrinsic membrane protein proton gradient regulation protein 5 (PGR5), were found to lack photosynthetic control [111]. This observation could be due to the important role of PGR5 in generating ΔpH via CET [114], alternatively it may have a direct effect on Q-cycle function [110] or possibly a combination of both [17] (see Section 9).

Irrespective of the precise control mechanism, the central role of cytb_6f in LET regulation is underlined by a flux control co-efficient in high light of 0.8 [121]. Indeed, overexpression of the ISP in *Arabidopsis* or the C4 plant *Setaria viridis* increases LET in high light [122,123], while its antisense inhibition reduces LET [124–127]. An additional limitation on cytb_6f turnover in high light might be the availability of PQ at the Q_n site, just as PQH_2 availability at Q_p may limit electron flow under low light (see below). This putative mechanism has been termed the reduction-induced suppression of electron flow (RISE) and there is some evidence for this operating in certain cyanobacteria [128,129]. The extent to which RISE is mitigated by the rapid exchange of PQ/PQH_2 between the Q_p and Q_n site [70](see Section 5) remains to be determined.

While in high light the activity of cytb_6f is limited by ΔpH, under low light it can instead be limited by the diffusion of PQ/PQH_2 from PSII through the protein-crowded membrane (e.g. 70-80% protein in spinach thylakoids) to the Q_p site [121,130,131]. In cyanobacteria, plants and algae, this diffusion limitation is somewhat mitigated by the co-localisation of PSII and cytb_6f complexes within nanodomains [21,132–135], which limits the average distance between the two complexes and lowers the mean diffusion time. Despite these measures, the effect of restricted diffusion is further exacerbated under low light where the ratio of PQ to PQH_2 is higher and thus competition between the two species for access to the Q_p binding pocket is increased (see Section 4). With this in mind, it is interesting to note that in higher plants the distance between the stromal pool of cytb_6f and PSII in the grana is significantly decreased under low light due to a reduction in grana diameter [132,136]. These changes in membrane architecture effectively shorten the diffusion distance between the two complexes, increasing the relative concentration of cytb_6f readily accessible to the LET pathway [132,137]. The associated decrease in grana diameter involved in this process is regulated by the phosphorylation of LHCII; which is mediated under low light by a cytb_6f-associated LHCII kinase (STN7) (see Section 10) [132,136,137]. A further demonstration of the importance of PQ/PQH_2 diffusion on the rate of cytb_6f activity was provided in recent genetic study by Cramer and co-workers, whereby, the entrance to the Q_p portal was further narrowed by mutation of residues in the F-helix of subIV (Pro105Ala and Pro112Ala in *Synechococcus* sp. PCC 7002 cytb_6f) [138]. These mutations were observed to slow the rate of cyt*f* reduction, resulting in an overall decreased growth rate relative to the WT. Given these observations, it is possible that a rational redesign to widen the Q_p portal might have the opposite effect, serving to accelerate the rate of cytb_6f activity and subsequently enhance growth, though this remains to be explored [50].

9. Does cytb_6f fulfil the role of the elusive ferredoxin-quinone reductase (FQR) involved in cyclic electron transfer?

While LET requires cooperation between the four major photosynthetic membrane protein complexes (PSII, cytb_6f, PSI, ATP synthase) to produce NADPH and ATP, CET returns electrons from Fd to the PQ/PQH_2 pool, forming a loop around cytb_6f and PSI [139,140](Fig 1). In this manner, *pmf* can be generated without net formation of reductant, allowing the relative production of ATP and NADPH to be fine-tuned to meet the varying metabolic demands of the cell [141,142]. Through generation of ΔpH, CET also plays a key role in the

599 control of light harvesting and photoprotection, enabling plants, algae and cyanobacteria to
600 adapt to environmental stress [139,140]. Two pathways of CET, involving two distinct
601 ferredoxin-quinone reductase (FQR) activities, occur in plants and cyanobacteria [143]. The
602 CET2 pathway (Fig 1) is provided by the protonmotive NDH-1 complex, which is related to
603 complex I in mitochondria [114,144–148]. In *Chlamydomonas*, NDH-1 is absent and instead
604 a non-protonmotive NDH-2 complex that utilises NADPH as an electron donor is found
605 [149]. In spinach and *Arabidopsis*, the major cyclic pathway is, unlike NDH-1, sensitive to
606 the inhibitor antimycin A (AA) [143,150]. AA is a known inhibitor of UQ reduction at the
607 cytbc_1 Q_n site [61,62], implicating the cytb_6f complex as the FQR for the CET1 pathway (Fig
608 1)[150]. This was further corroborated by kinetic evidence from Hind and co-workers,
609 showing haem b_p/b_n oxidation and the associated electrogenic reaction are affected by the
610 inhibition or enhancement of CET [9,151]. The idea that electrons could be donated directly
611 from Fd to cytb_6f is consistent with the original Q-cycle mechanism, suggested by Mitchell
612 [1], where the first electron for PQ reduction at the Q_n site is obtained from haem b_n and the
613 second may be provided by an n-side electron donor. Indeed, Hind *et al* suggested the
614 involvement of a co-factor 'V' in cytb_6f that would accept electrons from Fd and equilibrate
615 with the *b*-haems [9]. This idea was consistent with the characterisation of a high-spin *c*'-type
616 haem (termed 'G'), by Lavergne and Joliot, that was thought to be located on a soluble
617 protein associated with the stromal side of cytb_6f in the green alga *Chlorella* [64,152]. Co-
618 purification of cytb_6f with ferredoxin-$NADP^+$ reductase (FNR) [12,153], which was
619 previously shown to be essential for AA-sensitive CET [154,155], suggested the two
620 complexes might cooperate to form the CET1 FQR [10,12,156]. The discovery of haem c_n on
621 the stromal side of cytb_6f in 2003 provided a straightforward route for this transfer and it was
622 shown that haem c_n was the previously identified 'G' haem [40,41]. However, the finding
623 that the Q_n site in cytb_6f is insensitive to inhibition with AA, led to an alternative suggestion
624 that another protein may perform the role of the elusive AA-sensitive FQR [63].
625 The later discovery of the involvement of the PGR5 and PGRL1 (or Ssr2016 and
626 Sll1217, respectively, in cyanobacteria) proteins in CET therefore led to the suggestion that
627 they may form a separate FQR enzyme [157–159]. Indeed, PGR5 was shown to be the AA-
628 sensitive component [159,160]. This view was corroborated by the demonstration that PGR5
629 and PGRL1 could together facilitate the AA-sensitive reduction of 2,6-dimethoxy-1,4-
630 benzoquinone (DMBQ) in the presence of Fd, FNR and NADPH without requirement for
631 cytb_6f [159]. However, the rate of DMBQ reduction by the PGR5-PGRL1-FNR-Fd-NADPH
632 mixture was very slow, with a half-time in the range of seconds [159], which is incompatible

with the high rates of CET observed *in vivo* (~ 60 and 120 $e^- s^{-1}$ in *Chlamydomonas* and *Arabidopsis* respectively)[161–163]. Moreover, several studies in *Arabidopsis* and *Chlamydomonas* suggest that PGR5 and PGRL1 perform an indirect, regulatory role in CET [164,165]. Therefore one possibility is that PGRL1 and PGR5 might regulate the association of a supercomplex containing cytb_6f, PSI and FNR [10,154,158] and indeed such a complex was isolated from *Chlamydomonas* [166–168]. A supercomplex of this type was suggested to promote CET by sequestering PQ and Pc and thereby compartmentalising these components to avoid competition with LET [166]. However, in higher plants, where thylakoid stacking is stricter and more extensive than in *Chlamydomonas*, separation of cytb_6f in granal and stromal lamellae pools may achieve the same compartmentalisation of LET and CET without the need for a supercomplex [132,169]. The regulatory overlap between STN7/STT7-dependent phosphorylation and CET is further discussed in Section 10 below.

Recently, Q-cycle operation has been shown to be defective in the *pgr5* mutant in *Chlamydomonas* under CET-stimulating anoxic conditions [17]. Specifically, while an increased *b*-haem oxidation rate is observed under anoxic compared to oxic conditions in the wild-type, this increase is absent in the *pgr5* mutant. Since PGR5 is known to affect the tethering of FNR to the thylakoid in *Chlamydomonas* [170], the authors proposed that FNR binding to cytb_6f mediates CET1 via a Fd-assisted Q-cycle [17]. Building on these ideas a hypothetical Fd-assisted Q-cycle scheme is proposed in Figure 12. In the Fd-assisted Q-cycle, Fd-FNR bound to cytb_6f would reduce the stromal accessible haem c_n and allow binding of PQ at the Q_n site (Fig 12A). The subsequent oxidation of PQH_2 at the Q_p site leads electron bifurcation between the high (Fig 12B) and low (Fig 12C) potential chains with haem *f* and b_n being reduced. The presence of the haem b_n^{red} / c_n^{red} pair would then allow the quasi-concerted double reduction of PQ at the Qn site to PQH_2 (Fig 12D). Thus, the Fd-assisted Q-cycle allows PQH_2 formation at the Q_n with a single turnover of the Q_p site. A possible redox scheme for this Fd-assisted Q-cycle is shown in Fig 12E. In this scenario the redox potential of haem c_n is shifted to a lower potential by an allosteric effect of Fd-FNR binding. Such a downshift in haem c_n potential would decrease the equilibrium constant for its reduction by haem b_n, thus allowing electrons derived from Fd-FNR to compete. Such a downshift in haem cn potential would decrease the equilibrium constant for its reduction by haem bn, thus allowing electrons derived from Fd-FNR to compete. However, we suggest that the slow reduction of the b-haems by Fd-FNR observed in vitro, is ameliorated in vivo through precise tethering of FNR-Fd to cytb_6f by PGR5 [171, 172, 173].

10. The role of cytb_6f in transmembrane signalling and mediating gene expression

The cytb_6f complex occupies the position of the 'halfway house' in photosynthetic electron transfer and thus holds a unique vantage to sense the redox state of both the PQ and the Pc pools (and perhaps that of the NADPH and Fd pools, seesee Section 9). These signals contain unique information on the relative rates of electron transport through PSI and PSII, the ATP/NADPH balance and, therefore, the prevailing environmental and metabolic conditions faced by the organism. Among the various mechanisms that enable an organism to adapt to changing conditions is the regulation of photosynthetic gene expression (e.g. changing the relative stoichiometries of PSI and PSII). Control of this fundamental mechanism relies on sensor kinases to sense redox-derived signals and trigger post-translational and transcriptional control events [174–176]. In higher plants and green algae, the 68 kDa serine/threonine LHCII kinase (STN7 in plants; STT7 in *Chlamydomonas*) is associated with cytb_6f [177–179]. STN7 phosphorylates the stromal-facing N-terminus of the light-harvesting complex II (LHCII) trimer subunits Lhcb1 and Lhcb2 [174,175,180], in addition to a range of other proteins involved in chloroplast protein translation and transcriptional control [181]. Phosphorylation of LHCII weakens the lateral and stacking interactions between the stromal faces of these complexes that underpin stacking of the thylakoid membrane into grana [132,136,182,183]. The increased repulsion between LHCII trimers reduces grana stacking and diameter while promoting dissociation from PSII and interaction with PSI (state transitions) [184]. State transitions are a key short-term regulatory response to rebalance the input of excitation energy between PSI and PSII [185,186] thereby controlling the relative efficiency of LET and CET, and ensuring redox homeostasis in the electron transfer chain and ATP/NADPH balance in the stroma [187,188]. Indeed, in *Chlamydomonas* STT7 also phosphorylates subIV and the CET effector protein PetO, which is absent in higher plants [189,190]. One possibility is that STT7-dependent phosphorylation may enhance CET in *Chlamydomonas* by reorganising the Q_n site to facilitate access of stromal electrons to haem c_n. While maximal CET activity does not strictly depend on STN7/ STT7-dependent phosphorylation when studied in the absence of LET [161,167,191], it may be important under conditions of competition between CET and LET, when the former is limited by PSI excitation e.g. under low light [192]. In contrast, under high light CET appears to be in competition with LET for oxidised PQ and here the reversal of STN7-dependent phosphorylation via the action of the TAP38/PPH1 phosphatase was essential for full CET

699 activity [132,192]. In addition to this short-term role, STN7/STT7 is also involved in the
700 long-term dynamic acclimation response that adjusts the stoichiometry of the various
701 components of the photosynthetic electron transfer chain in response to changing
702 environmental and metabolic conditions [191]. Indeed, it has been observed that plants
703 lacking STN7 are unable to acclimate to changing light conditions, while those lacking state
704 transitions alone due to a separate defect in LHCII binding to PSI remain unaffected [193].
705 While these crucial roles of STN7/STT7 have been elucidated, the exact mechanism of its
706 activation (and inactivation) remain unclear.
707 Given the activation of STN7/STT7 is known to rely upon the oxidation of PQH_2 by
708 cytb_6f, it is believed that this protein kinase forms a close association with the cytb_6f complex
709 near to the Q_p site on the lumenal side of the membrane [177,178]. While the structure of the
710 stromal kinase domain of STT7 from the alga *Micromonas* is available [194], the critical
711 transmembrane and a small N-terminal domain strctures have yet to be solved. It has been
712 proposed that the N-terminal domain of STN7/STT7 interacts with cytb_6f via the ISP and
713 subIV (helices F and G) [16,81,195–197](Fig 13). These putative interactions between cytb_6f
714 and STN7/STT7 are proposed to be catalytically essential, as observed by a study in which
715 this putative binding interface is disrupted through the expression of a chimeric subIV with
716 an extra TM helix; such chimera mutants were unable to undergo state transitions despite no
717 apparent change in the activity of cytb_6f [198].
718 Exactly how the interactions between STN7/STT7 and cytb_6f may occur, and the precise
719 mechanism of signal transmission from the Q_p site of cytb_6f to the n-side by STN7/STT7, are
720 currently unclear. STN7 possesses two catalytically essential cysteine residues (Cys68 and
721 73) located near the N-terminus. While these two residues reside outside of the kinase
722 domain and are located on the opposite side of the membrane to the substrate LHCII,
723 mutation of either of these residues abolishes kinase activity and inhibits state transitions
724 [196]. It is possible that, while these two residues may have no direct role in catalysis, they
725 may be involved in the activation of the kinase through the formation of disulphide bridges,
726 with the possible involvement of Q_p-generated superoxide [199]. Another possibility for
727 STN7/STT7 activation involves the phytyl tail of the Chl *a* in cytb_6f. Here it is proposed that
728 the isoprenoid tail may 'sense' the occupancy of the Q_p site and this signal may be transduced
729 to STN7/STT7 via the interaction between the Chl *a* macrocyclic ring and the F and G
730 helices of subIV where the kinase is proposed to bind [81,82,198].
731 Recently, a mutagenesis study in *Chlamydomonas* described an additional crucial
732 interaction between the kinase domain of STT7 and the stromal loop linking helices F and G

of the cytb_6f subIV [16]. Here it was observed that a number of residues in the stromal loop (Asn122, Tyr124 and Arg125) between the F and G helices are crucial for state transitions, with STT7 kinase activity being completely abolished when these residues are mutated. The importance of the *fg*-loop of cytb_6f in the potential interaction with STT7 is further corroborated by evidence from yeast two-hybrid assays, in which it was found that cytb_6f interacts with a region of STT7 corresponding to residues 244-379 and that this interaction was dependent on Arg125 of subIV of cytb_6f [16](Fig 13). It is interesting to note that these cytb_6f residues are highly conserved, with the exception of Tyr124 which is substituted by Phe in several species including spinach, *M. laminosus* and *Nostoc*. While the primary interaction and activation of STT7 appear to depend on its interaction with the stromal *fg*-loop of cytb_6f, the release of STT7 from this putative docking site may depend on signals associated with substrate occupancy and subsequent oxidation at the Q_p site. Arg125 may facilitate the switch between STT7 bound and unbound states in response to PQH_2 binding to Q_p, which could be conveyed through conformational changes in the F and G TMHs. Such conformational changes could break interactions between Arg125 and STT7 and allow it to form a close association with the C-terminus of cytb_6 via Leu215, thereby releasing STT7 [16] (Fig 13).

Just as the mechanism of STN7/STT7 activation remains unclear, its mechanism of inactivation also remains enigmatic. It is assumed that STN7/STT7 spontaneously reverts to an inactive form and must be periodically triggered to reactivate by cytb_6f [197]. Yet, in high light, despite more frequent turnover of PQH2 at the Qp site, STN7 is inhibited by the concurrent build-up of ΔpH [200] and/ or reduced thioredoxin [201]. It has been observed that the CET1 inhibitor AA prevents the inhibition of STN7 [202] and more recently that plants lacking PGR5 can also maintain kinase activity in high light [203]. These results suggest that STN7 inhibition may also be linked to the conformation and occupancy of the Q_n site of cytb_6f. In line, with this hypothesis we observed that Arg125 of subIV adopts two different conformations in the PQ occupied and unoccupied halves of the spinach cytb6f dimer [23]. In the PQ occupied half Arg125 forms a close interaction with Leu215 at the C-terminus of cytb_6, while in the unoccupied half it is rotated ~20° away towards the aqueous phase of the stroma (Fig. 13).

11. Conclusion.

The last decade has seen great leaps in our understanding of how cytb_6f fulfils its role as the orchestrator of photosynthetic electron transfer, coordinating both short and long-term

acclimation to a changing light environment. Yet equally, many questions remain; in particular- does cytb_6f show a large-scale movement of the ISP during catalysis as in cytbc_1? How is FNR associated with cytb_6f ? What role do PGR5 and PGRL1 play in facilitating CET1? What is the precise role of the chlorophyll molecule at the Q_p site? How is STN7/ STT7 bound to cytb_6f and how is it activated/ inactivated? Providing answers will require a coordinated effort blending molecular genetics and high-resolution structural biology with advanced spectroscopic methods. Hopefully the next few years will see cytb_6f yield its remaining secrets and in doing so enrich our understanding of oxygenic photosynthesis still further.

Acknowledgments

M.P.J. acknowledges funding from the Leverhulme Trust grant RPG-2016-161 and RPG-2019-045. C.N.H., A.H., and M.P.J. also gratefully acknowledge financial support from the Biotechnology and Biological Sciences Research Council (BBSRC UK), award numbers BB/M000265/1 and BB/P002005/1. LAM was supported by a BBSRC White Rose DTP studentship.

References:

[1] P. Mitchell, The protonmotive Q cycle: A general formulation, FEBS Lett., 59 (1975) 137–139.

[2] D. V. Dibrova, D.N. Shalaeva, M.Y. Galperin, A.Y. Mulkidjanian, Emergence of cytochrome bc complexes in the context of photosynthesis, Physiol. Plant., 161 (2017) 150–170.

[3] W.A. Cramer, S.S. Hasan, E. Yamashita, The Q cycle of cytochrome bc complexes: A structure perspective, Biochim. Biophys. Acta - Bioenerg., 7 (2011) 788–802.

[4] A.N. Tikhonov, The cytochrome b6f complex at the crossroad of photosynthetic electron transport pathways, Plant Physiol. Biochem., 81 (2014) 163–183.

[5] P.R. Rich, The quinone chemistry of bc complexes, Biochim. Biophys. Acta - Bioenerg., 1658 (2004) 165–171.

[6] A.Y. Mulkidjanian, Ubiquinol oxidation in the cytochrome bc1 complex: Reaction mechanism and prevention of short-circuiting, Biochim. Biophys. Acta - Bioenerg., 1709 (2005) 5–34.

[7] D.M. Kramer, W. Nitschke, J.W. Cooley, The Cytochrome bc 1 and Related bc Complexes: The Rieske/Cytochrome b Complex as the Functional Core of a Central Electron/Proton Transfer Complex, in: Purple Phototrophic Bact., 2009: pp. 451–473.

[8] J.L. Cape, M.K. Bowman, D.M. Kramer, Understanding the cytochrome bc complexes by what they don't do The Q-cycle at 30, Trends Plant Sci., 11 (2006) 46–55.

[9] D. Crowther, G. Hind, Partial characterization of cyclic electron transport in intact chloroplasts, Arch. Biochem. Biophys., 204 (1980) 568–577.

[10] P. Joliot, A. Joliot, Quantification of cyclic and linear flows in plants, Proc. Natl. Acad. Sci. U. S. A., 102 (2005) 4913–4918.

[11] W.J. Nawrocki, B. Bailleul, D. Picot, P. Cardol, F. Rappaport, F.A. Wollman, P. Joliot,

The mechanism of cyclic electron flow, Biochim. Biophys. Acta - Bioenerg., 1860 (2019) 433–438.
[12] H. Zhang, J.P. Whitelegge, W.A. Cramer, Ferredoxin:NADP+ Oxidoreductase Is a Subunit of the Chloroplast Cytochrome b6f Complex, J. Biol. Chem., 276 (2001) 38159–38165.
[13] G. Finazzi, J. Minagawa, G.N. Johnson, The Cytochrome b 6 f Complex: A Regulatory Hub Controlling Electron Flow and the Dynamics of Photosynthesis?, in: Cytochrome Complexes Evol. Struct. Energy Transduction, Signal., 2016: pp. 437–452.
[14] J.F. Allen, Cytochrome b6 f: structure for signalling and vectorial metabolism, Trends Plant Sci., 9 (2004) 130–137.
[15] M. Sarewicz, L. Bujinowicz, S. Bhaduri, S. Singh, W.A. Cramer, A. Osyczka, Metastable radical state, nonreactive with oxygen, is inherent to catalysis by respiratory and photosynthetic cytochromes bc1/b6f, Proc. Natl. Acad. Sci. U. S. A., 114 (2017) 1323–1328.
[16] L. Dumas, F. Zito, S. Blangy, P. Auroy, X. Johnson, G. Peltier, J. Alric, A stromal region of cytochrome b6f subunit IV is involved in the activation of the Stt7 kinase in Chlamydomonas, Proc. Natl. Acad. Sci. U. S. A., 114 (2017) 12063–12068.
[17] F. Buchert, L. Mosebach, P. Gäbelein, M. Hippler, PGR5 is required for efficient Q cycle in the cytochrome b6f complex during cyclic electron flow, Biochem. J., 477 (2020) 1631–1650.
[18] S.S. Hasan, E. Yamashita, D. Baniulis, W.A. Cramer, Quinone-dependent proton transfer pathways in the photosynthetic cytochrome b6f complex, Proc. Natl. Acad. Sci. U. S. A., 110 (2013) 4297–4302.
[19] A. Malnoë, F.A. Wollman, C. De Vitry, F. Rappaport, Photosynthetic growth despite a broken Q-cycle, Nat. Commun., 2 (2011) 301.
[20] G.E. Mayneord, C. Vasilev, L.A. Malone, D.J.K. Swainsbury, C.N. Hunter, M.P. Johnson, Single-molecule study of redox control involved in establishing the spinach plastocyanin-cytochrome b6f electron transfer complex, Biochim. Biophys. Acta - Bioenerg., 1860 (2019) 591–599.
[21] M.P. Johnson, C. Vasilev, J.D. Olsen, C.N. Hunter, Nanodomains of cytochrome b6f and photosystem II complexes in spinach grana thylakoid membranes, Plant Cell, 26 (2014) 3051–3061.
[22] S.S. Hasan, W.A. Cramer, Internal lipid architecture of the hetero-oligomeric cytochrome b 6f complex, Structure, (2014).
[23] L.A. Malone, P. Qian, G.E. Mayneord, A. Hitchcock, D.A. Farmer, R.F. Thompson, D.J.K. Swainsbury, N.A. Ranson, C.N. Hunter, M.P. Johnson, Cryo-EM structure of the spinach cytochrome b 6 f complex at 36 Å resolution, Nature, 575 (2019) 535–539.
[24] D. Stroebel, Y. Choquet, J.-L. Popot, D. Picot, An atypical haem in the cytochrome b6f complex, Nature, 426 (2003) 413–418.
[25] D. Baniulis, E. Yamashita, J.P. Whitelegge, A.I. Zatsman, M.P. Hendrich, S.S. Hasan, C.M. Ryan, W.A. Cramer, Structure-function, stability, and chemical modification of the cyanobacterial cytochrome b6f complex from Nostoc sp PCC 7120, J. Biol. Chem., 284 (2009) 9861–9869.
[26] G. Kurisu, H. Zhang, J.L. Smith, W.A. Cramer, Structure of the Cytochrome b6f Complex of Oxygenic Photosynthesis: Tuning the Cavity, Science (80-.)., 302 (2003) 1009–1014.
[27] J. Yan, G. Kurisu, W.A. Cramer, Intraprotein transfer of the quinone analogue inhibitor 2,5-dibromo-3-methyl-6-isopropyl-p-benzoquinone in the cytochrome b6f complex, Proc. Natl. Acad. Sci. U. S. A., (2006).

[28] E. Yamashita, H. Zhang, W.A. Cramer, Structure of the Cytochrome b6f Complex: Quinone Analogue Inhibitors as Ligands of Heme cn, J. Mol. Biol., 370 (2007) 39–52.
[29] S.S. Hasan, E.A. Proctor, E. Yamashita, N. V. Dokholyan, W.A. Cramer, Traffic within the cytochrome b6f lipoprotein complex: Gating of the quinone portal, Biophys. J., 107 (2014) 1620–1628.
[30] S.S. Hasan, J.T. Stofleth, E. Yamashita, W.A. Cramer, Lipid-induced conformational changes within the cytochrome b 6 f complex of oxygenic photosynthesis, Biochemistry, 52 (2013) 2649–2654.
[31] D. Xia, C.A. Yu, H. Kim, J.Z. Xia, A.M. Kachurin, L. Zhang, L. Yu, J. Deisenhofer, Crystal structure of the cytochrome bc1 complex from bovine heart mitochondria, Science (80-.)., 277 (1997) 60–66.
[32] L. Esser, M. Elberry, F. Zhou, C.A. Yu, L. Yu, D. Xia, Inhibitor-complexed structures of the cytochrome bc1 from the photosynthetic bacterium Rhodobacter sphaeroides, J. Biol. Chem., 283 (2008) 2846–2857.
[33] Z. Zhang, L. Huang, V.M. Shulmeister, Y.I. Chi, K.K. Kim, L.W. Hung, A.R. Crofts, E.A. Berry, S.H. Kim, Electron transfer by domain movement in cytochrome bc1, Nature, 392 (1998) 677–684.
[34] C. Lemaire, J. Girard-Bascou, F.A. Wollman, P. Bennoun, Studies on the cytochrome b6/f complex I Characterization of the complex subunits in Chlamydomonas reinhardtii, BBA - Bioenerg., 851 (1986) 229–238.
[35] S. Rexroth, D. Rexroth, S. Veit, N. Plohnke, K.U. Cormann, M.M. Nowaczyk, M. Rögner, Functional characterization of the small regulatory subunit PetP from the cytochrome b6f complex in Thermosynechococcus elongatus, Plant Cell, 26 (2014) 3435–3448.
[36] A.R. Crofts, S.W. Meinhardt, A Q-cycle mechanism for the cyclic electron-transfer chain of Rhodopseudomonas sphaeroides, Biochem. Soc. Trans., 10 (1982) 201–203.
[37] A.R. Crofts, S.W. Meinhardt, K.R. Jones, M. Snozzi, The role of the quinone pool in the cyclic electron-transfer chain of Rhodopseudomonas sphaeroides A modified Q-cycle mechanism, BBA - Bioenerg., 723 (1983) 202–218.
[38] B.R. Velthuys, A third site of proton translocation in green plant photosynthetic electron transport, Proc. Natl. Acad. Sci. U. S. A., 75 (1978) 6031–6034.
[39] R.E. Slovacek, D. Crowther, G. Hind, CYTOCHROME FUNCTION IN THE CYCLIC ELECTRON TRANSPORT PATHWAY OF CHLOROPLASTS, Biochim. Biophys. Acta - Bioenerg., 547 (1979) 138–148.
[40] J. Alric, Y. Pierre, D. Picot, J. Lavergne, F. Rappaport, Spectral and redox characterization of the heme Ci of the cytochrome b6f complex, Proc. Natl. Acad. Sci. U. S. A., 102 (2005) 15860–15865.
[41] F. Zito, J. Alric, Heme c i or c n of the Cytochrome b 6 f Complex, A Short Retrospective, in: Cytochrome Complexes Evol. Struct. Energy Transduction, Signal., 2016: pp. 295–306.
[42] E. Dolan, G. Hind, Kinetics of the reduction and oxidation of cytochromes b6 and *f* in isolated chloroplasts, BBA - Bioenerg., 357 (1974) 380–385.
[43] C.C. Page, C.C. Moser, X. Chen, P.L. Dutton, Natural engineering principles of electron tunnelling in biological oxidation-reduction, Nature, 402 (1999) 47–52.
[44] J. Yan, W.A. Cramer, Functional insensitivity of the cytochrome b6f complex to structure changes in the hinge region of the Rieske iron-sulfur protein, J. Biol. Chem., 278 (2003) 20925–20933.
[45] E. Darrouzet, M. Valkova-Valchanova, C.C. Moser, P.L. Dutton, F. Daldal, Uncovering the [2Fe2S] domain movement in cytochrome bc1 and its implications for energy conversion, Proc. Natl. Acad. Sci. U. S. A., 97 (2000) 4567–4572.

908 [46] S. Heimann, M.V. Ponamarev, W.A. Cramer, Movement of the Rieske Iron-Sulfur
909 Protein in the p-Side Bulk Aqueous Phase: Effect of Lumenal Viscosity on Redox
910 Reactions of the Cytochrome b6f Complex, Biochemistry, 39 (2000) 2692–2699.
911 [47] C. Breyton, Conformational Changes in the Cytochrome b6f Complex Induced by
912 Inhibitor Binding, J. Biol. Chem., 275 (2000) 13195–13201.
913 [48] B. Schoepp, M. Brugna, A. Riedel, W. Nitschke, D.M. Kramer, The Q(o)-site inhibitor
914 DBMIB favours the proximal position of the chloroplast Rieske protein and induces a
915 pK-shift of the redox-linked proton, FEBS Lett., 450 (1999) 245–250.
916 [49] G.M. Soriano, L.W. Guo, C. De Vitry, T. Kallas, W.A. Cramer, Electron transfer from
917 the Rieske iron-sulfur protein (ISP) to cytochrome f in vitro: Is a guided trajectory of
918 the ISP necessary for competent docking?, J. Biol. Chem., 277 (2002) 41865–41871.
919 [50] S. Saif Hasan, W.A. Cramer, On rate limitations of electron transfer in the
920 photosynthetic cytochrome b6f complex, Phys. Chem. Chem. Phys., 14 (2012) 13853–
921 13860.
922 [51] A.R. Crofts, B. Barquera, R.B. Gennis, R. Kuras, M. Guergova-Kuras, E.A. Berry,
923 Mechanism of ubiquinol oxidation by the bc1 complex: Different domains of the
924 quinol binding pocket and their role in the mechanism and binding of inhibitors,
925 Biochemistry, 38 (1999) 15807–15826.
926 [52] L. Esser, B. Quinn, Y.F. Li, M. Zhang, M. Elberry, L. Yu, C.A. Yu, D. Xia,
927 Crystallographic studies of quinol oxidation site inhibitors: A modified classification
928 of inhibitors for the cytochrome bc1 complex, J. Mol. Biol., 341 (2004) 281–302.
929 [53] F. Zito, G. Finazzi, P. Joliot, F.-A. Wollman, Glu78, from the Conserved PEWY
930 Sequence of Subunit IV, Has a Key Function in Cytochrome b6f Turnover,
931 Biochemistry, 37 (1998) 10395–10403.
932 [54] A.R. Crofts, S. Hong, N. Ugulava, B. Barquera, R. Gennis, M. Guergova-Kuras, E.A.
933 Berry, Pathways for proton release during ubihydroquinone oxidation by the bc1
934 complex, Proc. Natl. Acad. Sci. U. S. A., (1999).
935 [55] S. Izrailev, A.R. Crofts, E.A. Berry, K. Schulten, Steered molecular dynamics
936 simulation of the Rieske subunit motion in the cytochrome bc1 complex, Biophys. J.,
937 (1999).
938 [56] G. Finazzi, Redox-coupled proton pumping activity in cytochrome b6f, as evidenced
939 by the pH dependence of electron transfer in whole cells of Chlamydomonas
940 reinhardtii, Biochemistry, 41 (2002) 7475–7482.
941 [57] F. Baymann, F. Giusti, D. Picot, W. Nitschke, The ci/bH moiety in the b6f complex
942 studied by EPR: A pair of strongly interacting hemes, Proc. Natl. Acad. Sci. U. S. A.,
943 104 (2007) 519–524.
944 [58] H. Zhang, A. Primak, J. Cape, M.K. Bowma, D.M. Kramer, W.A. Cramer,
945 Characterization of the high-spin heme x in the cytochrome b6f complex of oxygenic
946 photosynthesis, Biochemistry, 43 (2004) 16329–16336.
947 [59] A. de Lacroix de Lavalette, L. Barucq, J. Alric, F. Rappaport, F. Zito, Is the Redox
948 State of the ci Heme of the Cytochrome b6f Complex Dependent on the Occupation
949 and Structure of the Qi Site and Vice Versa?, J. Biol. Chem., 284 (2009) 20822–
950 20829.
951 [60] E.A. Berry, M. Guergova-Kuras, L.S. Huang, A.R. Crofts, Structure and function of
952 cytochrome bc complexes, Annu. Rev. Biochem., 69 (2000) 1005–1075.
953 [61] E.C. Slater, The mechanism of action of the respiratory inhibitor, antimycin, BBA
954 Rev. Bioenerg., 301 (1973) 129–154.
955 [62] M.K.F. Wikström, J.A. Berden, Oxidoreduction of cytochrome b in the presence of
956 antimycin, Biochim. Biophys. Acta - Bioenerg., 283 (1972) 403–420.
957 [63] D.A. Moss, D.S. Bendall, Cyclic electron transport in chloroplasts The Q-cycle and the

site of action of antimycin, Biochim. Biophys. Acta - Bioenerg., 767 (1984) 389–395.
[64] J. Lavergne, Membrane potential-dependent reduction of cytochrome b-6 in an algal mutant lacking Photosystem I centers, BBA - Bioenerg., 725 (1983) 25–33.
[65] D. Xia, L. Esser, L. Yu, C.A. Yu, Structural basis for the mechanism of electron bifurcation at the quinol oxidation site of the cytochrome bc1 complex, Photosynth. Res., 92 (2007) 17–34.
[66] X. Gao, X. Wen, L. Esser, B. Quinn, L. Yu, C.A. Yu, D. Xia, Structural basis for the quinone reduction in the bc1 complex: A comparative analysis of crystal structures of mitochondrial cytochrome bc1 with bound substrate and inhibitors at the Qi site, Biochemistry, (2003).
[67] R.P. Barbagallo, C. Breyton, G. Finazzi, Kinetic effects of the electrochemical proton gradient on plastoquione reduction at the Qi site of the cytochrome b6f complex, J. Biol. Chem., 275 (2000) 26121–26127.
[68] C. Klughammer, S. Heimann, U. Schreiber, Inhibition of cytochrome b563-oxidation by triorganotins in spinach chloroplasts, Photosynth. Res., 56 (1998) 117–130.
[69] M. Swierczek, E. Cieluch, M. Sarewicz, A. Borek, C.C. Moser, P.L. Dutton, A. Oszycka, An Electronic Bus Bar Lies in the Core of Cytochrome bc1, Science (80-.)., 329 (2010) 451–454.
[70] P. Joliot, A. Joliot, Mechanism of proton-pumping in the cytochrome b/f complex, Photosynth. Res., (1986) 113–124.
[71] J.L. Cape, M.K. Bowman, D.M. Kramer, Computation of the redox and protonation properties of quinones: Towards the prediction of redox cycling natural products, Phytochemistry, 67 (2006) 1781–1788.
[72] A. Osyczka, C.C. Moser, P.L. Dutton, Fixing the Q cycle, Trends Biochem. Sci., 30 (2005) 176–182.
[73] D. Baniulis, S. Saif Hasan, I. Miliute, W.A. Cramer, Mechanisms of Superoxide Generation and Signaling in Cytochrome bc Complexes, in: Cytochrome Complexes Evol. Struct. Energy Transduction, Signal., 2016: pp. 397–417.
[74] J.L. Cape, M.K. Bowman, D.M. Kramer, A semiquinone intermediate generated at the Qo site of the cytochrome bc1 complex: Importance for the Q-cycle and superoxide production, Proc. Natl. Acad. Sci. U. S. A., 104 (2007) 7887–7892.
[75] E. Berry, H. LS, Observations concerning the quinol oxidation site of the cytochrome bc1 complex, FEBS Lett., 555 (2003) 13–20.
[76] Y. Pierre, C. Breyton, D. Kramer, J.L. Popot, Purification and characterization of the cytochrome b6 f complex from Chlamydomonas reinhardtii, J. Biol. Chem., 270 (1995) 29342–29349.
[77] D. Huang, R.M. Everly, R.H. Cheng, J.B. Heymann, T.S. Baker, W.A. Cramer, H. Schägger, V. Sled, T. Ohnishi, Characterization of the Chloroplast Cytochrome b6f Complex as a Structural and Functional Dimer, Biochemistry, 33 (1994) 4401–4409.
[78] E.J.G. Peterman, S.O. Wenk, T. Pullerits, L.O. Pålsson, R. Van Grondelle, J.P. Dekker, M. Rögner, H. Van Amerongen, Fluorescence and absorption spectroscopy of the weakly fluorescent chlorophyll a in cytochrome b6f of Synechocystis PCC6803, Biophys. J., 75 (1998) 389–398.
[79] N. Dashdorj, H. Zhang, H. Kim, J. Yan, W.A. Cramer, S. Savikhin, The single chlorophyll a molecule in the cytochrome b6 f complex: Unusual optical properties protect the complex against singlet oxygen, Biophys. J., 88 (2005) 4178–4187.
[80] J. Yan, N. Dashdorj, D. Baniulis, E. Yamashita, S. Savikhin, W.A. Cramer, On the structural role of the aromatic residue environment of the chlorophyll a in the cytochrome b6f complex, Biochemistry, 47 (2008) 3654–3661.
[81] A.D.L. De Lavalette, G. Finazzi, F. Zito, b6f-associated chlorophyll: Structural and

dynamic contribution to the different cytochrome functions, Biochemistry, 47 (2008) 5259–5265.
[82] S.S. Hasan, E. Yamashita, W.A. Cramer, Transmembrane signaling and assembly of the cytochrome b6f-lipidic charge transfer complex, Biochim. Biophys. Acta - Bioenerg., 1827 (2013) 1295–1308.
[83] A. Torrado, C. Ramírez-Moncayo, J.A. Navarro, V. Mariscal, F.P. Molina-Heredia, Cytochrome c6 is the main respiratory and photosynthetic soluble electron donor in heterocysts of the cyanobacterium Anabaena sp PCC 7120, Biochim. Biophys. Acta - Bioenerg., 1860 (2019) 60–68.
[84] E.L. Gross, Plastocyanin: structure and function, Photosynth. Res., 37 (1993) 103–116.
[85] W. Haehnel, A. Propper, H. Krause, Evidence for complexed plastocyanin as the immediate electron donor of P-700, Biochim. Biophys. Acta - Bioenerg., 593 (1980) 384–399.
[86] A.B. Hope, Electron transfers amongst cytochrome f, plastocyanin and photosystem I: Kinetics and mechanisms, Biochim. Biophys. Acta - Bioenerg., 1456 (2000) 5–26.
[87] M. Ubbink, The courtship of proteins: Understanding the encounter complex, FEBS Lett., 583 (2009) 1060–1066.
[88] I. Díaz-Moreno, A. Díaz-Quintana, M.A. De la Rosa, M. Ubbink, Structure of the Complex between Plastocyanin and Cytochrome f from the Cyanobacterium Nostoc sp PCC 7119 as Determined by Paramagnetic NMR, J. Biol. Chem., 280 (2005) 18908–18915.
[89] J. Illerhaus, L. Altschmied, J. Reichert, E. Zak, R.G. Herrmann, W. Haehnel, Dynamic Interaction of Plastocyanin with the Cytochrome bf Complex , J. Biol. Chem. , 275 (2000) 17590–17595.
[90] X.-S. Gong, J.Q. Wen, N.E. Fisher, S. Young, C.J. Howe, D.S. Bendall, J.C. Gray, The role of individual lysine residues in the basic patch on turnip cytochrome f for electrostatic interactions with plastocyanin in vitro, Eur. J. Biochem., 267 (2000) 3461–3468.
[91] B. Hyun Lee, T. Hibino, T. Takabe, P.J. Weisbeek, T. Takabe, Site-Directed Mutagenetic Study on the Role of Negative Patches on Silene Plastocyanin in the Interactions with Cytochrome f and Photosystem I1, J. Biochem., 117 (1995) 1209–1217.
[92] S. Modi, M. Nordling, L.G. Lundberg, Ö. Hansson, D.S. Bendall, Reactivity of cytochromes c and f with mutant forms of spinach plastocyanin, Biochim. Biophys. Acta - Bioenerg., 1102 (1992) 85–90.
[93] T. Ueda, N. Nomoto, M. Koga, H. Ogasa, Y. Ogawa, M. Matsumoto, P. Stampoulis, K. Sode, H. Terasawa, I. Shimada, Structural Basis of Efficient Electron Transport between Photosynthetic Membrane Proteins and Plastocyanin in Spinach Revealed Using Nuclear Magnetic Resonance, Plant Cell, 24 (2012) 4173 LP – 4186.
[94] M. Ubbink, M. Ejdebäck, B.G. Karlsson, D.S. Bendall, The structure of the complex of plastocyanin and cytochrome f, determined by paramagnetic NMR and restrained rigid-body molecular dynamics, Structure, (1998).
[95] S.E. Hart, B.G. Schlarb-Ridley, C. Delon, D.S. Bendall, C.J. Howe, Role of Charges on Cytochrome f from the Cyanobacterium Phormidium laminosum in Its Interaction with Plastocyanin, Biochemistry, 42 (2003) 4829–4836.
[96] I. Díaz-Moreno, A. Díaz-Quintana, M.A. De La Rosa, P.B. Crowley, M. Ubbink, Different modes of interaction in cyanobacterial complexes of plastocyanin and cytochrome f, Biochemistry, 44 (2005) 3176–3183.
[97] L. Qin, N.M. Kostic, Importance of protein rearrangement in the electron-transfer reaction between the physiological partners cytochrome f and plastocyanin,

Biochemistry, 32 (1993) 6073–6080.
[98] P.B. Crowley, N. Vintonenko, G.S. Bullerjahn, M. Ubbink, Plastocyanin−Cytochrome f Interactions: The Influence of Hydrophobic Patch Mutations Studied by NMR Spectroscopy, Biochemistry, 41 (2002) 15698–15705.
[99] S. Ramos, A.L. Le Sueur, R.E. Horness, J.T. Specker, J.A. Collins, K.E. Thibodeau, M.C. Thielges, Heterogeneous and Highly Dynamic Interface in Plastocyanin–Cytochrome f Complex Revealed by Site-Specific 2D-IR Spectroscopy, J. Phys. Chem. B, 123 (2019) 2114–2122.
[100] W.M. Kaiser, H. Weber, M. Sauer, Photosynthetic Capacity, Osmotic Response and Solute Content of Leaves and Chloroplasts From Spinacia oleracea Under Salt Stress, Zeitschrift Für Pflanzenphysiologie, 113 (1983) 15–27.
[101] S. Izawa, N.E. Good, Effect of Salts and Electron Transport on the Conformation of Isolated Chloroplasts II Electron Microscopy, Plant Physiol., 41 (1966) 544 LP – 552.
[102] G.M. Soriano, M. V Ponamarev, G.-S. Tae, W.A. Cramer, Effect of the Interdomain Basic Region of Cytochrome f on Its Redox Reactions in Vivo, Biochemistry, 35 (1996) 14590–14598.
[103] G.M. Soriano, M. V Ponamarev, R.A. Piskorowski, W.A. Cramer, Identification of the Basic Residues of Cytochrome f Responsible for Electrostatic Docking Interactions with Plastocyanin in Vitro: Relevance to the Electron Transfer Reaction in Vivo, Biochemistry, 37 (1998) 15120–15128.
[104] A. Singharoy, A.M. Barragan, S. Thangapandian, E. Tajkhorshid, K. Schulten, Binding Site Recognition and Docking Dynamics of a Single Electron Transport Protein: Cytochrome c2, J. Am. Chem. Soc., 138 (2016) 12077–12089.
[105] K.R. West, J.T. Wiskich, Photosynthetic control by isolated pea chloroplasts, Biochem. J., 109 (1968) 527–532.
[106] B. Rumberg, E. Reinwald, H. Schröder, U. Siggel, Correlation between electron flow, proton translocation and phosphorylation in chloroplasts, Naturwissenschaften, 55 (1968) 77–79.
[107] H.H. Stiehl, H.T. Witt, Quantitative Treatment of the Function of Plastoquinone in Photosynthesis*, Zeitschrift Fur Naturforsch. - Sect. B J. Chem. Sci., 24 (1969) 1588–1598.
[108] C.A. Sacksteder, A. Kanazawa, M.E. Jacoby, D.M. Kramer, The proton to electron stoichiometry of steady-state photosynthesis in living plants: A proton-pumping Q cycle is continuously engaged, Proc. Natl. Acad. Sci. U. S. A., 97 (2000) 14283–14288.
[109] C. Miyake, Molecular mechanism of oxidation of p700 and suppression of ROS production in photosystem I in response to electron-sink limitations in C3 plants, Antioxidants, 9 (2020) 230.
[110] M. Suorsa, M. Grieco, S. Järvi, P.J. Gollan, S. Kangasjärvi, M. Tikkanen, E.M. Aro, PGR5 ensures photosynthetic control to safeguard photosystem I under fluctuating light conditions, Plant Signal. Behav., (2013) e22741.
[111] M. Suorsa, S. Järvi, M. Grieco, M. Nurmi, M. Pietrzykowska, M. Rantala, S. Kangasjärvi, V. Paakkarinen, M. Tikkanen, S. Jansson, E.M. Aro, PROTON GRADIENT REGULATION5 is essential for proper acclimation of Arabidopsis photosystem I to naturally and artificially fluctuating light conditions, Plant Cell, 24 (2012) 2934–2948.
[112] R. Barbato, L. Tadini, R. Cannata, C. Peracchio, N. Jeran, A. Alboresi, T. Morosinotto, A.A. Bajwa, V. Paakkarinen, M. Suorsa, E.M. Aro, P. Pesaresi, Higher order photoprotection mutants reveal the importance of ΔpH-dependent photosynthesis-control in preventing light induced damage to both photosystem II and photosystem I,

Sci. Rep., 10 (2020) 1.
[113] K. Sonoike, Photoinhibition of photosystem I, Physiol. Plant., 142 (2011) 56–64.
[114] Y. Munekage, M. Hashimoto, C. Miyake, K.I. Tomizawa, T. Endo, M. Tasaka, T. Shikanai, Cyclic electron flow around photosystem I is essential for photosynthesis, Nature, 429 (2004) 579–582.
[115] T.J. Avenson, J.A. Cruz, A. Kanazawa, D.M. Kramer, Regulating the proton budget of higher plant photosynthesis, Proc. Natl. Acad. Sci. U. S. A., 102 (2005) 9709–9713.
[116] P. Jahns, M. Graf, Y. Munekage, T. Shikanai, Single point mutation in the Rieske iron-sulfur subunit of cytochrome b6/f leads to an altered pH dependence of plastoquinol oxidation in Arabidopsis, FEBS Lett., 519 (2002) 99–102.
[117] H. Yamamoto, T. Shikanai, PGR5-dependent cyclic electron flow protects photosystem I under fluctuating light at donor and acceptor sides, Plant Physiol., 179 (2019) 588–600.
[118] D.M. Kramer, C.A. Sacksteder, J.A. Cruz, How acidic is the lumen?, Photosynth. Res., 60 (1999) 151–163.
[119] S. Hald, B. Nandha, P. Gallois, G.N. Johnson, Feedback regulation of photosynthetic electron transport by NADP(H) redox poise, Biochim. Biophys. Acta - Bioenerg., 1777 (2008) 433–440.
[120] G.N. Johnson, Thiol regulation of the thylakoid electron transport chain - A missing link in the regulation of photosynthesis?, Biochemistry, 42 (2003) 3040–3044.
[121] H. Kirchhoff, S. Horstmann, E. Weis, Control of the photosynthetic electron transport by PQ diffusion microdomains in thylakoids of higher plants, Biochim. Biophys. Acta - Bioenerg., 1459 (2000) 148–168.
[122] A.J. Simkin, L. McAusland, T. Lawson, C.A. Raines, Overexpression of the rieskeFeS protein increases electron transport rates and biomass yield, Plant Physiol., 175 (2017) 134–145.
[123] M. Ermakova, P.E. Lopez-Calcagno, C.A. Raines, R.T. Furbank, S. von Caemmerer, Overexpression of the Rieske FeS protein of the Cytochrome b6f complex increases C4 photosynthesis, Commun. Biol., 314 (2019).
[124] V. Hurry, J.M. Anderson, M.R. Badger, G.D. Price, Reduced levels of cytochrome b6/f in transgenic tobacco increases the excitation pressure on photosystem II without increasing sensitivity to photoinhibition in vivo, Photosynth. Res., 50 (1996) 159–169.
[125] J.M. Anderson, G.D. Price, W.S. Chow, A.B. Hope, M.R. Badger, Reduced levels of cytochrome bf complex in transgenic tobacco leads to marked photochemical reduction of the plastoquinone pool, without significant change in acclimation to irradiance, Photosynth. Res., 53 (1997) 215–227.
[126] G.D. Price, S. Von Caemmerer, J.R. Evans, K. Siebke, J.M. Anderson, M.R. Badger, Photosynthesis is strongly reduced by antisense suppression of chloroplastic cytochrome bf complex in transgenic tobacco, Aust. J. Plant Physiol., 25 (1998) 445–452.
[127] W. Yamori, S. Takahashi, A. Makino, G.D. Price, M.R. Badger, S. von Caemmerer, The roles of ATP synthase and the cytochrome b6/f complexes in limiting chloroplast electron transport and determining photosynthetic capacity, Plant Physiol., 155 (2011) 956–962.
[128] K. Shaku, G. Shimakawa, M. Hashiguchi, C. Miyake, Reduction-Induced Suppression of Electron Flow (RISE) in the Photosynthetic Electron Transport System of Synechococcus elongatus PCC 7942, Plant Cell Physiol., 57 (2015) 1443–1453.
[129] G. Shimakawa, K. Shaku, C. Miyake, Reduction-induced suppression of electron flow (RISE) is relieved by non-ATP-consuming electron flow in Synechococcus elongatus PCC 7942, Front. Microbiol., 9 (2018) 886.

[130] I.G. Tremmel, H. Kirchhoff, E. Weis, G.D. Farquhar, Dependence of plastoquinol diffusion on the shape, size, and density of integral thylakoid proteins, Biochim. Biophys. Acta - Bioenerg., 1607 (2003) 97–109.
[131] P. Joliot, J. Lavergne, D. Béal, Plastoquinone compartmentation in chloroplasts I Evidence for domains with different rates of photo-reduction, Biochim. Biophys. Acta - Bioenerg., 1101 (1992) 1–12.
[132] W.H.J. Wood, C. MacGregor-Chatwin, S.F.H. Barnett, G.E. Mayneord, X. Huang, J.K. Hobbs, C.N. Hunter, M.P. Johnson, Dynamic thylakoid stacking regulates the balance between linear and cyclic photosynthetic electron transfer, Nat. Plants, 4 (2018) 116–127.
[133] C. MacGregor-Chatwin, M. Sener, S.F.H. Barnett, A. Hitchcock, M.C. Barnhart-Dailey, K. Maghlaoui, J. Barber, J.A. Timlin, K. Schulten, C.N. Hunter, Lateral segregation of photosystem i in cyanobacterial thylakoids, Plant Cell, 29 (2017) 1119–1136.
[134] L.-S. Zhao, T. Huokko, S. Wilson, D.M. Simpson, Q. Wang, A. V Ruban, C.W. Mullineaux, Y.-Z. Zhang, L.-N. Liu, Structural variability, coordination and adaptation of a native photosynthetic machinery, Nat. Plants, 6 (2020) 869–882.
[135] W. Wietrzynski, M. Schaffer, D. Tegunov, S. Albert, A. Kanazawa, J. Plitzko, W. Baumeister, B. Engel, Charting the native architecture of thylakoid membranes with single-molecule precision, Elife, 9 (2019) e53740.
[136] W.H.J. Wood, S.F.H. Barnett, S. Flannery, C.N. Hunter, M.P. Johnson, Dynamic thylakoid stacking is regulated by LHCII phosphorylation but not its interaction with PSI, Plant Physiol., 180 (2019) 2152–2166.
[137] L. Dumas, M. Chazaux, G. Peltier, X. Johnson, J. Alric, Cytochrome b 6 f function and localization, phosphorylation state of thylakoid membrane proteins and consequences on cyclic electron flow, Photosynth. Res., 129 (2016) 307–320.
[138] J. Ness, S. Naurin, K. Effinger, V. Stadnytskyi, I.M. Ibrahim, S. Puthiyaveetil, W.A. Cramer, Structure-based control of the rate limitation of photosynthetic electron transport, FEBS Lett., 593 (2019) 2103–2111.
[139] W. Yamori, T. Shikanai, Physiological Functions of Cyclic Electron Transport Around Photosystem I in Sustaining Photosynthesis and Plant Growth, Annu. Rev. Plant Biol., 67 (2016) 81–106.
[140] G.N. Johnson, Physiology of PSI cyclic electron transport in higher plants, Biochim. Biophys. Acta - Bioenerg., 1807 (2011) 384–389.
[141] C.H. Foyer, J. Neukermans, G. Queval, G. Noctor, J. Harbinson, Photosynthetic control of electron transport and the regulation of gene expression, J. Exp. Bot., 63 (2012) 1637–1661.
[142] D.M. Kramer, J.R. Evans, The Importance of Energy Balance in Improving Photosynthetic Productivity, Plant Physiol., 155 (2011) 70–78.
[143] T. Endo, H. Mil, T. Shikanai, K. Asada, Donation of Electrons to Plastoquinone by NAD(P)H Dehydrogenase and by Ferredoxin-Quinone Reductase in Spinach Chloroplasts, Plant Cell Physiol., 38 (1997) 1272–1277.
[144] T. Joët, L. Cournac, E.M. Horvath, P. Medgyesy, G. Peltier, Increased sensitivity of photosynthesis to antimycin a induced by inactivation of the chloroplast ndhB gene Evidence for a participation of the NADH-dehydrogenase complex to cyclic electron flow around photosystem I, Plant Physiol., 125 (2001) 1919–1929.
[145] A.K. Livingston, J.A. Cruz, K. Kohzuma, A. Dhingra, D.M. Kramer, An arabidopsis mutant with high cyclic electron flow around photosystem i (hcef) involving the nadphdehydrogenase complex, Plant Cell, 22 (2010) 221–233.
[146] D.D. Strand, N. Fisher, D.M. Kramer, The higher plant plastid NAD(P)H

dehydrogenase-like complex (NDH) is a high efficiency proton pump that increases ATP production by cyclic electron flow, J. Biol. Chem., 292 (2017) 11850–11860.
[147] J.M. Schuller, J.A. Birrell, H. Tanaka, T. Konuma, H. Wulfhorst, N. Cox, S.K. Schuller, J. Thiemann, W. Lubitz, P. Sétif, T. Ikegami, B.D. Engel, G. Kurisu, M.M. Nowaczyk, Structural adaptations of photosynthetic complex I enable ferredoxin-dependent electron transfer, Science (80-.)., 363 (2019) 257–260.
[148] T.G. Laughlin, A.N. Bayne, J.-F. Trempe, D.F. Savage, K.M. Davies, Structure of the complex I-like molecule NDH of oxygenic photosynthesis, Nature, 566 (2019) 411–414.
[149] F. Jans, E. Mignolet, P.-A. Houyoux, P. Cardol, B. Ghysels, S. Cuiné, L. Cournac, G. Peltier, C. Remacle, F. Franck, A type II NAD(P)H dehydrogenase mediates light-independent plastoquinone reduction in the chloroplast of Chlamydomonas, Proc. Natl. Acad. Sci., 105 (2008) 20546–20551.
[150] K. Tagawa, H.Y. Tsujimoto, D.I. Arnon, ROLE OF CHLOROPLAST FERREDOXIN IN THE ENERGY CONVERSION PROCESS OF PHOTOSYNTHESIS, Proc. Natl. Acad. Sci., 49 (1963) 567–572.
[151] R.E. Slovacek, D. Crowther, G. Hind, Cytochrome function in the cyclic electron transport pathway of chloroplasts, BBA - Bioenerg., 547 (1979) 138–148.
[152] P. Joliot, A. Joliot, The low-potential electron-transfer chain in the cytochrome bf complex, Biochim. Biophys. Acta - Bioenerg., 933 (1988) 319–333.
[153] R.D. Clark, M.J. Hawkesford, S.J. Coughlan, J. Bennett, G. Hind, Association of ferredoxin-NADP+ oxidoreductase with the chloroplast cytochrome b-f complex, FEBS Lett., 174 (1984) 137–142.
[154] P. Joliot, G.N. Johnson, Regulation of cyclic and linear electron flow in higher Plants, Proc. Natl. Acad. Sci. U. S. A., 108 (2011) 13317–13322.
[155] Y. Shahak, D. Crowther, G. Hind, The involvement of ferredoxin-NADP+ reductase in cyclic electron transport in chloroplasts, BBA - Bioenerg., 636 (1981) 234–243.
[156] H.C.P. Matthijs, R. Jeanjean, N. Yeremenko, J. Huisman, F. Joset, K.J. Hellingwerf, Hypothesis: Versatile function of ferredoxin-NADP+ reductase in cyanobacteria provides regulation for transient photosystem I-driven cyclic electron flow, Funct. Plant Biol., 29 (2002) 201–210.
[157] M. Dann, D. Leister, Evidence that cyanobacterial Sll1217 functions analogously to PGRL1 in enhancing PGR5-dependent cyclic electron flow, Nat. Commun., 10 (2019) 5299.
[158] G. DalCorso, P. Pesaresi, S. Masiero, E. Aseeva, D. Schünemann, G. Finazzi, P. Joliot, R. Barbato, D. Leister, A Complex Containing PGRL1 and PGR5 Is Involved in the Switch between Linear and Cyclic Electron Flow in Arabidopsis, Cell, 132 (2008) 273–285.
[159] A.P. Hertle, T. Blunder, T. Wunder, P. Pesaresi, M. Pribil, U. Armbruster, D. Leister, PGRL1 Is the Elusive Ferredoxin-Plastoquinone Reductase in Photosynthetic Cyclic Electron Flow, Mol. Cell, (2013).
[160] K. Sugimoto, Y. Okegawa, A. Tohri, T.A. Long, S.F. Covert, T. Hisabori, T. Shikanai, A Single Amino Acid Alteration in PGR5 Confers Resistance to Antimycin A in Cyclic Electron Transport around PSI, Plant Cell Physiol., 54 (2013) 1525–1534.
[161] J. Alric, Redox and ATP control of photosynthetic cyclic electron flow in Chlamydomonas reinhardtii: (II) Involvement of the PGR5-PGRL1 pathway under anaerobic conditions, Biochim. Biophys. Acta - Bioenerg., 1837 (2014) 825–834.
[162] P. Joliot, A. Joliot, Cyclic electron transfer in plant leaf, Proc. Natl. Acad. Sci. U. S. A., 99 (2002) 10209–10214.
[163] P. Joliot, D. Béal, A. Joliot, Cyclic electron flow under saturating excitation of dark-

1258 adapted Arabidopsis leaves, Biochim. Biophys. Acta - Bioenerg., (2004).
1259 [164] W.J. Nawrocki, B. Bailleul, P. Cardol, F. Rappaport, F.A. Wollman, P. Joliot,
1260 Maximal cyclic electron flow rate is independent of PGRL1 in Chlamydomonas,
1261 Biochim. Biophys. Acta - Bioenerg., 1860 (2019) 425–432.
1262 [165] B. Nandha, G. Finazzi, P. Joliot, S. Hald, G.N. Johnson, The role of PGR5 in the redox
1263 poising of photosynthetic electron transport, Biochim. Biophys. Acta - Bioenerg., 1767
1264 (2007) 1252–1259.
1265 [166] M. Iwai, K. Takizawa, R. Tokutsu, A. Okamuro, Y. Takahashi, J. Minagawa, Isolation
1266 of the elusive supercomplex that drives cyclic electron flow in photosynthesis, Nature,
1267 464 (2010) 1210–1213.
1268 [167] H. Takahashi, S. Clowez, F.A. Wollman, O. Vallon, F. Rappaport, Cyclic electron
1269 flow is redox-controlled but independent of state transition, Nat. Commun., 4 (2013)
1270 1954.
1271 [168] J. Steinbeck, I.L. Ross, R. Rothnagel, P. Gäbelein, S. Schulze, N. Giles, R. Ali, R.
1272 Drysdale, E. Sierecki, Y. Gambin, H. Stahlberg, Y. Takahashi, M. Hippler, B.
1273 Hankamer, Structure of a PSI-LHCI-cyt b6f supercomplex in Chlamydomonas
1274 reinhardtii promoting cyclic electron flow under anaerobic conditions, Proc. Natl.
1275 Acad. Sci. U. S. A., (2018).
1276 [169] P.Å. Albertsson, A quantitative model of the domain structure of the photosynthetic
1277 membrane, Trends Plant Sci., 6 (2001) 349–354.
1278 [170] L. Mosebach, C. Heilmann, R. Mutoh, P. Gäbelein, J. Steinbeck, T. Happe, T.
1279 Ikegami, G. Hanke, G. Kurisu, M. Hippler, Association of Ferredoxin:NADP+
1280 oxidoreductase with the photosynthetic apparatus modulates electron transfer in
1281 Chlamydomonas reinhardtii, Photosynth. Res., 134 (2017) 291–306.
1282 [171] P.C. Maxwell, J. Biggins, Role of Cyclic Electron Transport in Photosynthesis as
1283 Measured by the Photoinduced Turnover of P700 in Vivo, Biochemistry, 15 (1976)
1284 3975–3981.
1285 [172] P.N. Furbacher, M.E. Girvin, W.A. Cramer, On the Question of Interheme Electron
1286 Transfer in the Chloroplast Cytochrome b6 in Situ, Biochemistry, 28 (1989) 8990–
1287 8998.
1288 [173] R. Szymańska, J. Dłuzewska, I. Ślesak, J. Kruk, Ferredoxin:NADP + oxidoreductase
1289 bound to cytochrome b 6f complex is active in plastoquinone reduction: Implications
1290 for cyclic electron transport, Physiol. Plant., 141 (2011) 289–298.
1291 [174] N. Depège, S. Bellafiore, J.D. Rochaix, Role of chloroplast protein kinase Stt7 in
1292 LHCII phosphorylation and state transition in Chlamydomonas, Science (80-.)., 299
1293 (2003) 1572–1575.
1294 [175] S. Bellaflore, F. Barneche, G. Peltler, J.D. Rochalx, State transitions and light
1295 adaptation require chloroplast thylakoid protein kinase STN7, Nature, 433 (2005) 892–
1296 895.
1297 [176] S. Puthiyaveetil, T.A. Kavanagh, P. Cain, J.A. Sullivan, C.A. Newell, J.C. Gray, C.
1298 Robinson, M. van der Giezen, M.B. Rogers, J.F. Allen, The ancestral symbiont sensor
1299 kinase CSK links photosynthesis with gene expression in chloroplasts, Proc. Natl.
1300 Acad. Sci., 105 (2008) 10061 LP – 10066.
1301 [177] F. Zito, G. Finazzi, R. Delosme, W. Nitschke, D. Picot, F.-A. Wollman, The Qo site of
1302 cytochrome b6f complexes controls the activation of the LHCII kinase, EMBO J., 18
1303 (1999) 2961–2969.
1304 [178] A. V. Vener, P.J.M. Van Kan, P.R. Rich, I. Ohad, B. Andersson, Plastoquinol at the
1305 quinol oxidation site of reduced cytochrome bf mediates signal transduction between
1306 light and protein phosphorylation: Thylakoid protein kinase deactivation by a single-
1307 turnover flash, Proc. Natl. Acad. Sci. U. S. A., 94 (1997) 1585–1590.

[179] S. Lemeille, A. Willig, N. Depège-Fargeix, C. Delessert, R. Bassi, J.-D. Rochaix, Analysis of the Chloroplast Protein Kinase Stt7 during State Transitions, PLOS Biol., 7 (2009) e1000045.
[180] J.F. Allen, J. Bennett, K.E. Steinback, C.J. Arntzen, Chloroplast protein phosphorylation couples plastoquinone redox state to distribution of excitation energy between photosystems, Nature, 291 (1981) 25–29.
[181] A. Schönberg, A. Rödiger, W. Mehwald, J. Galonska, G. Christ, S. Helm, D. Thieme, P. Majovsky, W. Hoehenwarter, S. Baginsky, Identification of STN7/STN8 kinase targets reveals connections between electron transport, metabolism and gene expression, Plant J., 90 (2017) 1176–1186.
[182] D.J. Kyle, L.A. Staehelin, C.J. Arntzen, Lateral mobility of the light-harvesting complex in chloroplast membranes controls excitation energy distribution in higher plants, Arch. Biochem. Biophys., 222 (1983) 527–541.
[183] M. Pietrzykowska, M. Suorsa, D.A. Semchonok, M. Tikkanen, E.J. Boekema, E. Aro, S. Jansson, The Light-Harvesting Chlorophyll a / b Binding Proteins Lhcb1 and Lhcb2 Play Complementary Roles during State Transitions in Arabidopsis, 26 (2014) 3646–3660.
[184] L.A. Staehelin, C.J. Arntzen, Regulation of chloroplast membrane function: Protein phosphorylation changes the spatial organization of membrane components, J. Cell Biol., 97 (1983) 1327–1337.
[185] A. V. Ruban, M.P. Johnson, Dynamics of higher plant photosystem cross-section associated with state transitions, Photosynth. Res., 99 (2009) 173–183.
[186] M. Goldschmidt-Clermont, R. Bassi, Sharing light between two photosystems: Mechanism of state transitions, Curr. Opin. Plant Biol., 25 (2015) 71–78.
[187] J.F. Allen, Protein phosphorylation - Carburettor of photosynthesis?, Trends Biochem. Sci., 8 (1983) 369–373.
[188] P. Cardol, J. Alric, J. Girard-Bascou, F. Franck, F.A. Wollman, G. Finazzi, Impaired respiration discloses the physiological significance of state transitions in Chlamydomonas, Proc. Natl. Acad. Sci. U. S. A., 15 (2009) 15979–15984.
[189] S.V. Bergner, M. Scholz, K. Trompelt, J. Barth, P. Gäbelein, J. Steinbeck, H. Xue, S. Clowez, G. Fucile, M. Goldschmidt-Clermont, C. Fufezan, M. Hippler, STATE TRANSITION7-Dependent phosphorylation is modulated by changing environmental conditions, and its absence triggers remodeling of photosynthetic protein complexes, Plant Physiol., (2015).
[190] F. Buchert, M. Hamon, P. Gäbelein, M. Scholz, M. Hippler, F.A. Wollman, The labile interactions of cyclic electron flow effector proteins, J. Biol. Chem., (2018).
[191] P. Pesaresi, A. Hertle, M. Pribil, T. Kleine, R. Wagner, H. Strissel, A. Lhnatowicz, V. Bonardi, M. Scharfenberg, A. Schneider, T. Pfannschmidt, D. Leister, Arabidopsis STN7 kinase provides a link between short- and long-term photosynthetic acclimation, Plant Cell, 21 (2009) 2402–2423.
[192] C. Hepworth, W.H.J. Wood, T.Z. Emrich-Mills, M.S. Proctor, S. Casson, M.P. Johnson, Dynamic thylakoid stacking and state transitions work synergistically to avoid acceptor-side limitation of photosystem I, Nat. Plants, xxxx (2021) Doi: 10.1038/s41477-020-00828-3.
[193] M. Grieco, M. Tikkanen, V. Paakkarinen, S. Kangasjärvi, E.M. Aro, Steady-state phosphorylation of light-harvesting complex II proteins preserves photosystem I under fluctuating white light, Plant Physiol., 160 (2012) 1896–1910.
[194] J. Guo, X. Wei, M. Li, X. Pan, W. Chang, Z. Liu, Structure of the catalytic domain of a state transition kinase homolog from Micromonas algae, Protein Cell, 4 (2013) 607–619.

[195] S. Lemeille, M. V. Turkina, A. V. Vener, J.D. Rochaix, Stt7-dependent phosphorylation during state transitions in the green alga Chlamydomonas reinhardtii, Mol. Cell. Proteomics, 9 (2010) 1281–1295.
[196] A. Shapiguzov, X. Chai, G. Fucile, P. Longoni, L. Zhang, J.-D. Rochaix, Activation of the Stt7/STN7 Kinase through Dynamic Interactions with the Cytochrome b6f Complex, Plant Physiol., 171 (2016) 82–92.
[197] G. Finazzi, The central role of the green alga Chlamydomonas reinhardtii in revealing the mechanism of state transitions, J. Exp. Bot., 56 (2005) 383–388.
[198] F. Zito, J. Vinh, J.-L. Popot, G. Finazzi, Chimeric Fusions of Subunit IV and PetL in the b6f Complex of Chlamydomonas reinhardtii, J. Biol. Chem., 277 (2002) 12446–55.
[199] S.K. Singh, S.S. Hasan, S.D. Zakharov, S. Naurin, W. Cohn, J. Ma, J.P. Whitelegge, W.A. Cramer, Trans-membrane Signaling in Photosynthetic State Transitions: REDOX- AND STRUCTURE-DEPENDENT INTERACTION IN VITRO BETWEEN STT7 KINASE AND THE CYTOCHROME b6f COMPLEX , J. Biol. Chem. , 291 (2016) 21740–21750.
[200] P. Fernyhough, C.H. Foyer, P. Horton, Increase in the level of thylakoid protein phosphorylation in maize mesophyll chloroplasts by decrease in the transthylakoid pH gradient, FEBS Lett., 176 (1984) 133–138.
[201] E. Rintamäki, P. Martinsuo, S. Pursiheimo, E.M. Aro, Cooperative regulation of light-harvesting complex II phosphorylation via the plastoquinol and ferredoxin-thioredoxin system in chloroplasts, Proc. Natl. Acad. Sci. U. S. A., 97 (2000) 11644–11649.
[202] K. Oxborough, P. Lee, P. Horton, Regulation of thylakoid protein phosphorylation by high-energy-state quenching, FEBS Lett., 221 (1987) 211–214.
[203] N.R. Mekala, M. Suorsa, M. Rantala, E.M. Aro, M. Tikkanen, Plants actively avoid state transitions upon changes in light intensity: Role of light-harvesting complex ii protein dephosphorylation in high light, Plant Physiol., 168 (2015) 721–734.
[204] A.B. Hope, The chloroplast cytochrome bf complex A critical focus on function, BBA - Bioenerg., 1143 (1993) 1–22.
[205] H. Kirchhoff, M.A. Schöttler, J. Maurer, E. Weis, Plastocyanin redox kinetics in spinach chloroplasts: Evidence for disequilibrium in the high potential chain, Biochim. Biophys. Acta - Bioenerg., 1659 (2004) 63–72.
[206] S.R.N. Solmaz, C. Hunte, Structure of complex III with bound cytochrome C in reduced state and definition of a minimal core interface for electron transfer, J. Biol. Chem., (2008).
[207] Y. Xue, M. Ökvist, Ö. Hansson, S. Young, Crystal structure of spinach plastocyanin at 17 Å resolution, Protein Sci., (1998).
[208] G. Kurisu, M. Kusunoki, E. Katoh, T. Yamazaki, K. Teshima, Y. Onda, Y. Kimata-Ariga, T. Hase, Structure of the electron transfer complex between ferredoxin and ferredoxin-NAPD+ reductase, Nat. Struct. Biol., 8 (2001) 117–121.

Supplementary Data

Table 1 | The subunit composition of the cytochrome b_6f complex.

		Molecular Weight (kDa)[a]				
Subunit	Gene	*S. oleracea*	*C. reinhardtii*	*M. laminosus*	*Nostoc*	Associated Cofactor(s)
Cyt *f*	*petA*	31.32 (P16013)	31.25 (P23577)	32.30 (P83793)	31.15 (Q93SW9)	*c*-type haem (*f*)
Cyt b_6	*petB*	24.17 (P00165)	24.17 (Q00471)	24.23 (P83791)	24.27 (P0A384)	*b*-type haems (b_p and b_n)
ISP	*petC*	18.94 (P08980)	18.40 (P49728)	19.40 (P83794)	19.20 (Q93SX0)	[2Fe-2S] cluster
SubIV	*petD*	17.45 (P00166)	17.44 (P23230)	17.67 (P83792)	17.54 (Q93SX1)	Chl*a*, β-carotene
PetL	*petL*	3.45 (Q9M3L0)	4.88 (P50369)	3.50 (P83795)	3.25 (Q8YVQ2)	-
PetM	*petM*	3.77 (P80883)	4.04 (Q42496)	3.84 (P83796)	3.55 (POA3Y1)	-
PetG	*petG*	4.17 (P69461)	3.98 (Q08362)	4.02 (P83797)	4.00 (P58246)	-
PetN	*petN*	3.17 (P61045)	3.73 (P0C1D4)	3.28 (P83798)	3.23 (P61048)	-

[a] Based on sequence minus signal peptides, Uniprot IDs are shown in brackets below each value.

Cofactor	Ligation [a]	Covalent bonds	Em value (mV)[c]
c-type haems			
haem *f*	Y1/H25 (cyt *f*)	C21/C24 (cyt *f*)	+355
haem c_n	H_2O_b	C35 (cyt b_6)	+100/-150
b-type haems			
haem b_p	H86/H187 (cyt b_6)	-	-150
haem b_n	H100/H202 (cyt b_6)	-	-85
[2Fe-2S]	C107/H109/C125/H128 (ISP)	-	+310
β-carotene	-	-	-
Chlorophyll *a*	-	-	-

[a] Residues numbered according to the *S. oleracea* structure (PDB ID: 6RQF) [23].
[b] Not resolved in the *S. oleracea* structure but indicated by other previous structures.
[c] Midpoint potentials shown are for cofactors in the *S. oleracea* cytochrome b_6f complex measured at pH 7 [204,205]

Table 2 |A comparison of edge-to-edge cofactor distances (Å) in each half of the b_6f dimer from different species (6RQF[23], 1Q90[24], 2E74[26], 4OGQ[29]) and the bc_1 dimer from different species with the Rieske ISP in its distal (1BCC[33]) and proximal (3BCC[33], 2BCC[33], 1SQP[52]) positions.

PDB ID	6RQF	1Q90	2E74	4OGQ
Source	*S. oleracea*	*C. reinhardtii*	*M. laminosus*	*Nostoc sp. PCC 7120*
Resolution (Å)	3.58	3.10	3.00	2.5 0
Inhibitors *	-	TDS (Q_p)	-	-
Distances:				
b_n - c_n (Å)	4.7, 4.7	4.7, 4.7	4.7, 4.7	4.6, 4.6
b_n - b_p (Å)	12.1, 12.0	12.2, 12.2	12.2, 12.2	12.1, 12.1
b_p - b_p (Å)	15.3	15.1	15.2	15.3
b_p - [2Fe-2S] (Å)	25.6, 25.5	22.9, 22.9	25.5, 25.5	25.3, 25.3
[2Fe-2S] - f (Å)	25.9, 26.1	27.8, 27.8	26.2, 26.2	26.2, 26.2

PDB ID	1BCC (distal)	3BCC (proximal)	2BCC (proximal)	1SQP (proximal)
Source	*G. gallus*	*G. gallus*	*G. gallus*	*B. taurus*
Resolution (Å)	3.16	3.70	3.50	2.70
Inhibitors *	-	STG (Q_p), AMY (Q_n)	STG (Q_p)	MYX (Q_p)
Distances:				
b_n - b_p (Å)	12.4, 12.4	12.3, 12.3	12.2, 12.2	12.1, 12.1
b_p - b_p (Å)	14.2	14.5	13.8	13.6
b_p - [2Fe-2S] (Å)	28.1, 28.2	23.0, 23.1	22.2, 22.3	25.1, 24.9
[2Fe-2S] - c_1 (Å)	16.2, 16.4	27.1, 27.3	27.3, 27.4	27.0, 26.8

* Inhibitors are indicated by the abbreviations TDS (tridecylstigmatellin), STG (stigmatellin), AMY (antimycin) and MYX (myxothiazol).

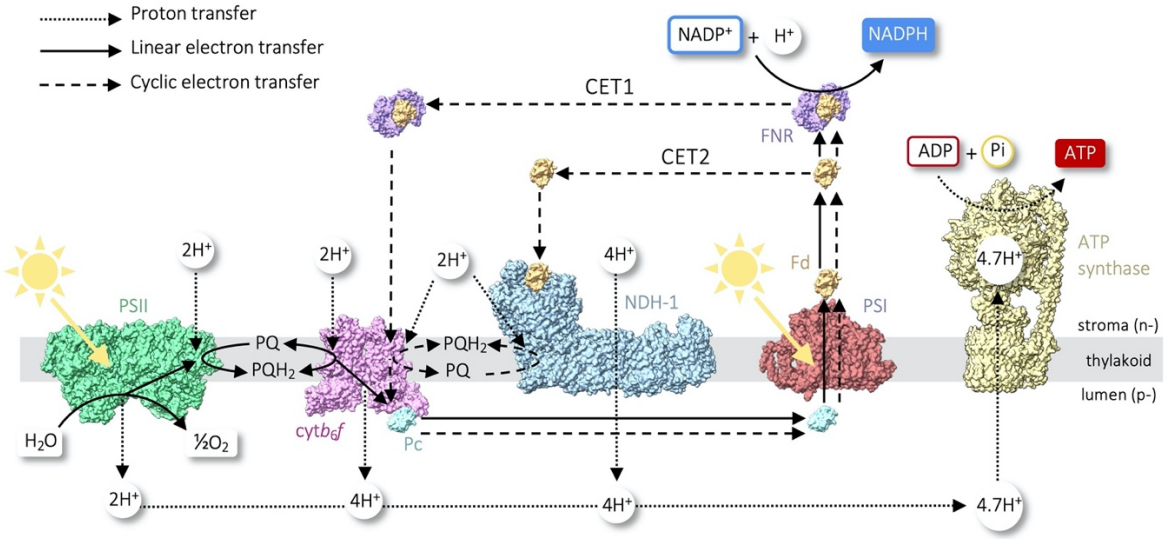

Fig. 1 | The photosynthetic electron and proton transfer chain. A schematic representation of the photosynthetic electron transfer chain showing components of the linear electron transfer (LET) pathway (solid black line) including photosystem II (PSII, green), cytochrome b_6f (cytb_6f, pink), plastocyanin (Pc, cyan), photosystem I (PSI, red), ferredoxin (Fd, dark yellow), the ferredoxin-NADP$^+$ reductase complex (FNR, purple) and ATP synthase (yellow). Additionally, the two proposed routes of cyclic electron transfer (CET) are also shown (dashed black lines): The CET1 pathway is mediated by PGRL1 and PGR5 (not shown) and involves the Fd-FNR complex, cytb_6f, Pc, PSI and ATP synthase; the CET2 pathway comprises the NADH dehydrogenase-like complex 1 (NDH-1, sky blue), cytb_6f, Pc, PSI and ATP synthase. The position of the lipid bilayer that separates the stromal (n-) and lumenal (p-) sides of the membrane is indicated by a grey stripe. Black dotted arrows indicate proton transfers in the LET and CET pathways. 4.7 H$^+$ are required per ATP synthesised by the ATP synthase.

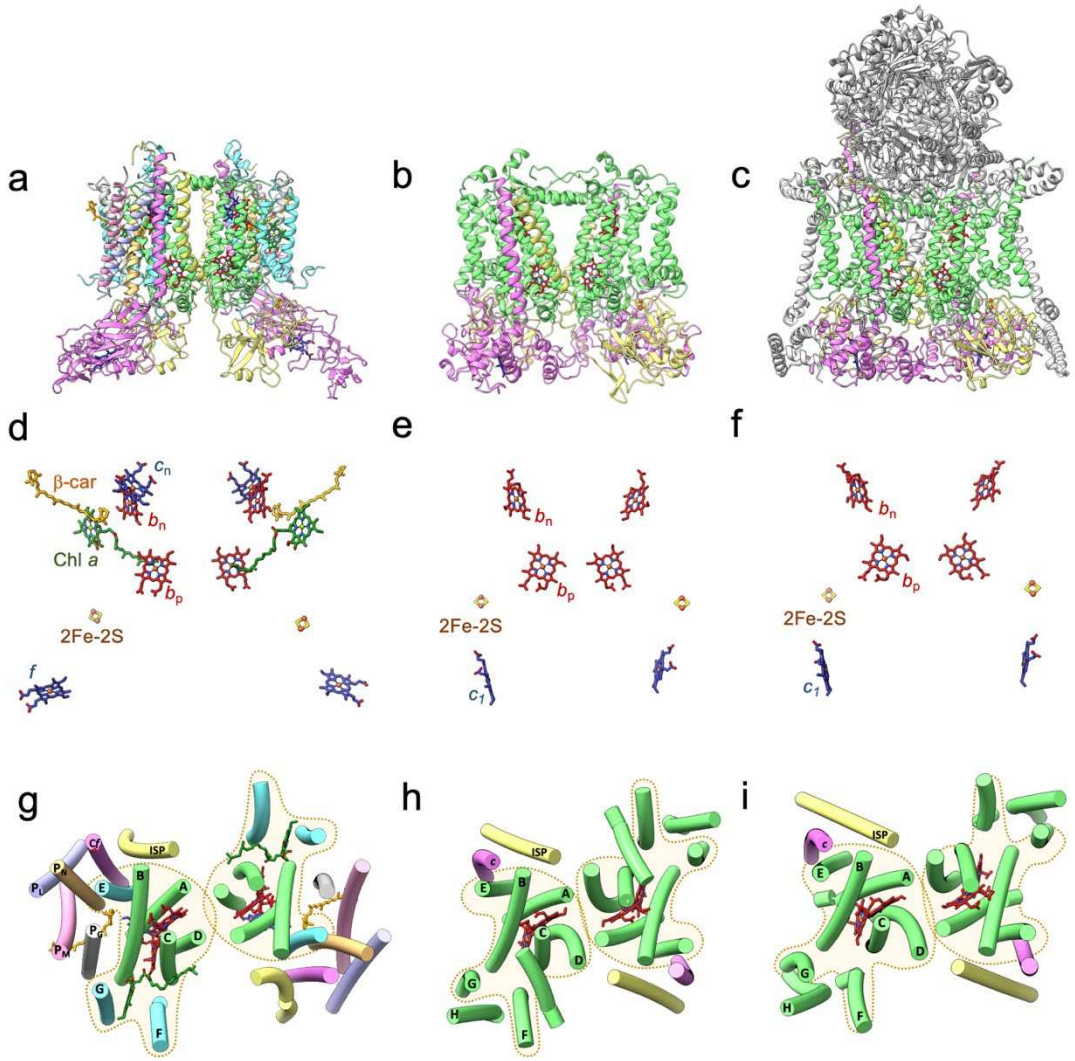

Fig. 2 | The similarities and differences between the cytochrome b_6f and bc_1 complexes. **a-c**, the polypeptide composition of: **a**, the cytb_6f complex (*S. oleracea*, 6RQF[23]) coloured with cytb_6 (green), cyt*f* (magenta), the ISP (yellow), subIV (cyan), PetG (grey), PetM (pink), PetN (pale orange) and PetL (pale purple); **b**, the bacterial cytbc_1 complex (*Rhodobacter sphaeroides*, 2QJP[32]) coloured with the ISP (yellow), cyt*b* (green) and cytc_1 (magenta); **c**, the mitochondrial cytbc_1 complex (*M. musculus*, 3CX5[206]) coloured with the ISP (yellow), cyt*b* (green), cytc_1 (magenta) and additional peripheral subunits (grey). **d-f**, the global arrangements of prosthetic groups within complexes shown in panels a-c with c-type haems (*f*, c_n and c_1; dark blue), *b*-type haems (b_p and b_n, red), Chl *a* (dark green), β-carotene (β-car - orange) and the 2Fe-2S cluster (S coloured yellow and Fe coloured red-orange). **g-i**, the arrangement of TM helices within complexes shown in panels a-c viewed perpendicular to the membrane plane from the p-side of the membrane (extrinsic domains, loops and additional non-conserved subunits in the bc_1 complexes are not shown for clarity).

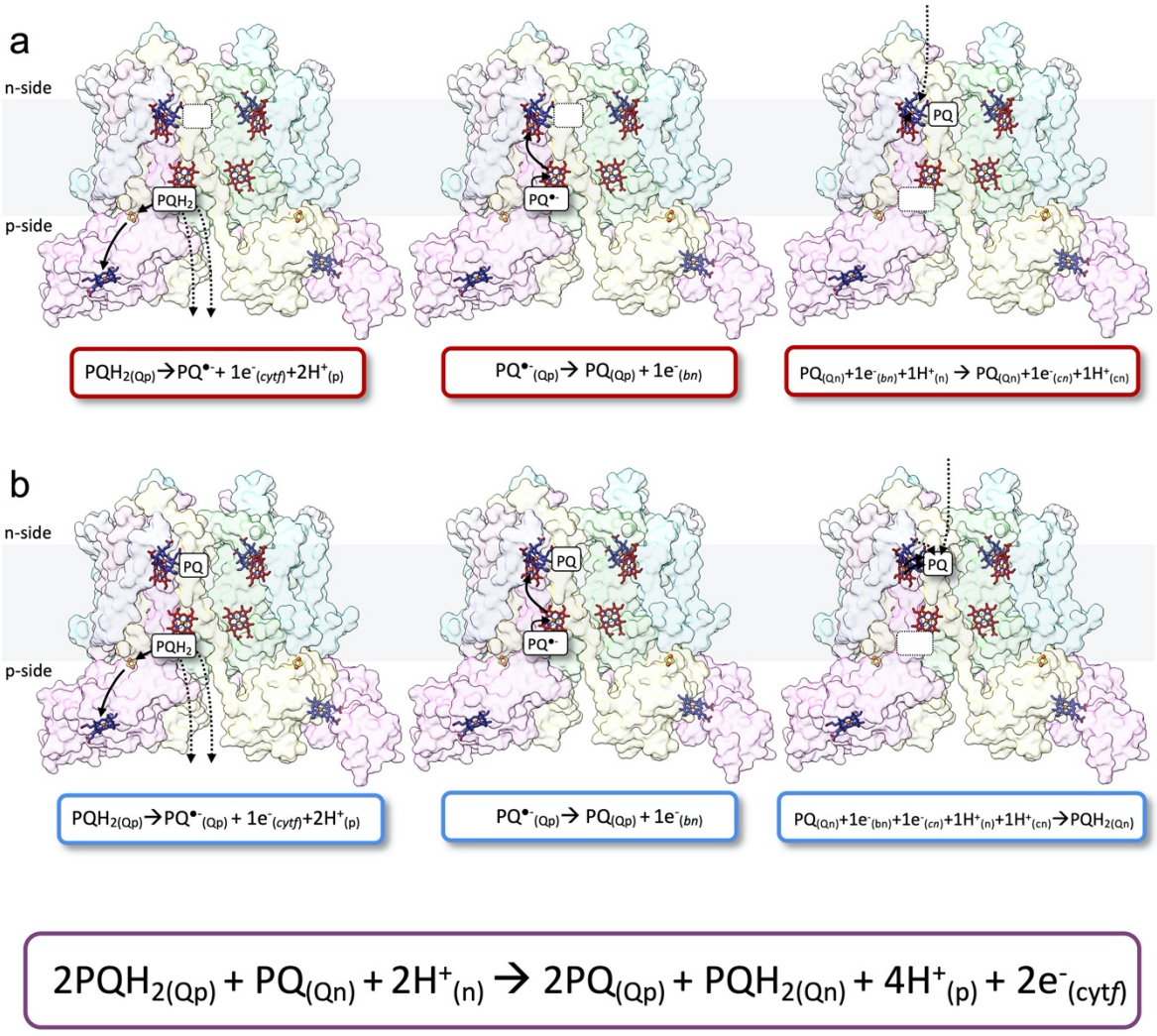

Fig. 3 | The proton motive Q-cycle of cytochrome b_6f. A schematic representation of the Q-cycle model for electron and proton transfer through the cytb_6f complex (*S. oleracea*, 6RQF[23]) based on the original cycle proposed by Mitchell [1] with modifications proposed by Crofts [21,22]. **a-b,** The cycle in cytb_6f is split into two half-cycles with **a,** showing each reaction step of the first half-cycle overlaid on the structure and summarised below in a red

box and **b,** showing each reaction step of the second half-cycle overlaid on the structure and summarised below in a blue box. The complete reaction is outlined below in the purple box. The position of the lipid bilayer that separates the stromal (n-) and lumenal (p-) sides of the membrane is indicated by a grey stripe. The Q_p and Q_n sites are denoted by a white box overlaid on the structure with a solid outline indicating the site is occupied by substrate while a black dashed outline indicates the site is empty. Black dotted arrows indicate proton transfers while solid black arrows indicate electron transfers. Subunits and prosthetic groups are coloured as in Fig 2A. **c**, Redox potential diagram of the cofactors involved in the Q-cycle. Midpoint potentials shown are those defined for the higher plants [204,205].

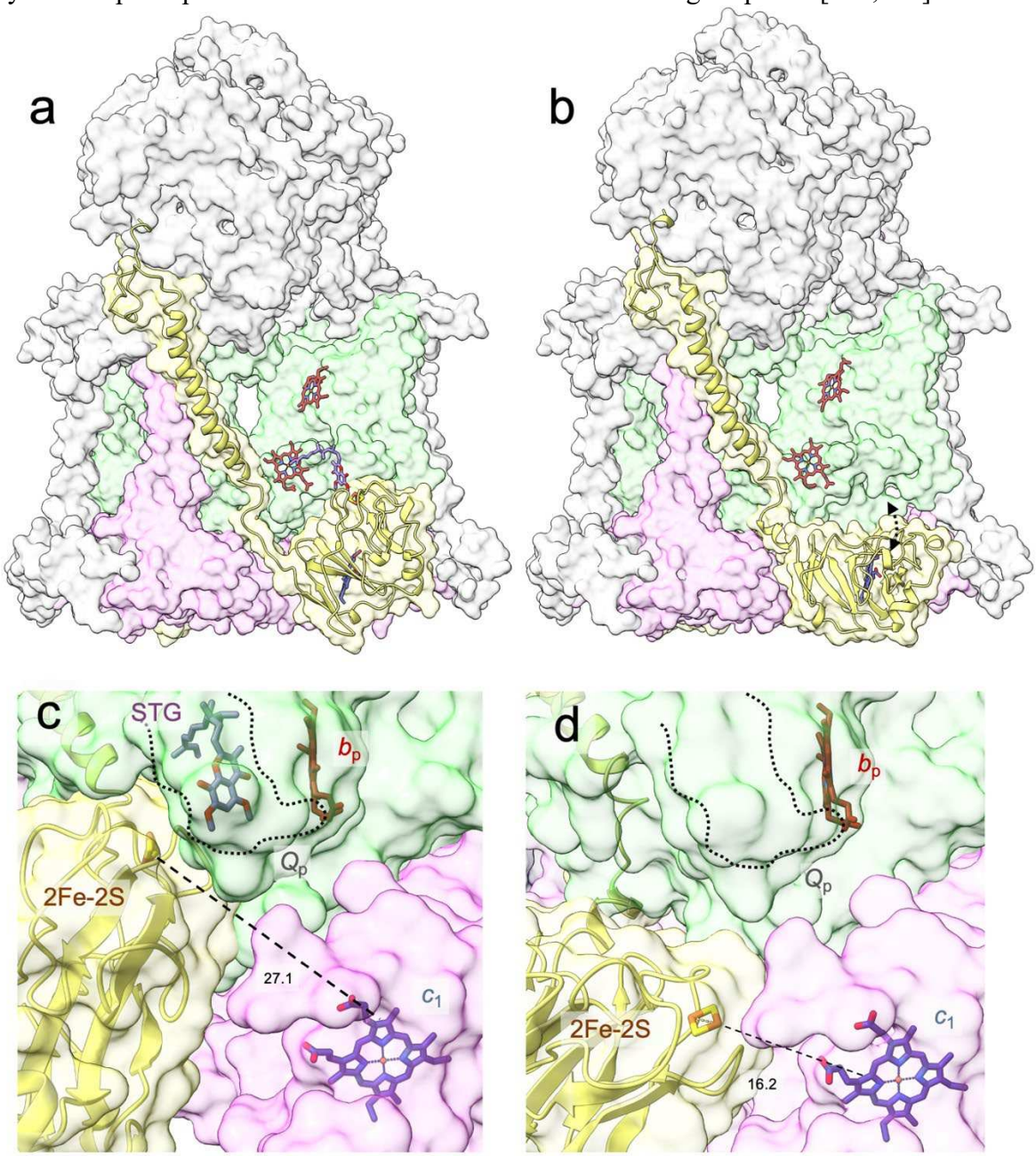

Fig. 4 | Large scale conformational changes occurring within the extrinsic domain of the ISP underlie catalysis in the cytochrome *bc*$_1$ complex. a-b, two conformations of the ISP are observed in the *G. gallus* cytochrome bc_1, the Q_p proximal position (a, 3BCC[33]) and the Q_p distal position (b, 1BCC) with an arrow indicating the scale of movement undergone by the 2Fe-2S cofactor. A video of the conformational change undergone by the Rieske subunit

depicted in panel b is provided in the supplementary material online. **c-d**, a close-up view of a-b showing the relative distances between cofactors in the Q_p proximal position (c, 3BCC) and the Q_p distal position (d, 1BCC[33]). Distances are indicated by a black dashed line with the distance indicated below in (Å). Prosthetic groups are shown in stick representation beneath a semi-transparent protein surface, additionally a ribbon representation of the Rieske protein is shown. An outline of the Q_p site is also indicated by a grey dotted line. Subunits and prosthetic groups are coloured as in Fig 2A.

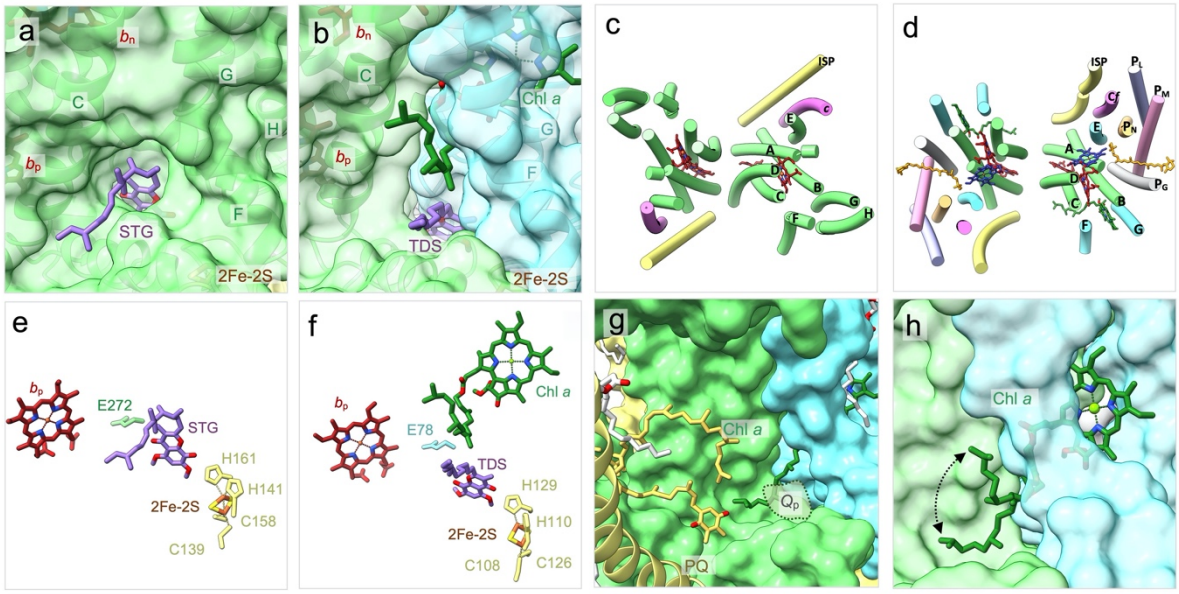

Fig. 5 | The Q_p sites of cytbc_1 and cytb_6f. a-b, a surface view of the Q_p site in the cytbc_1 complex from *G. gallus* (a, 3BCC[33]) and the cytb_6f complex from *Mastigocladus laminosus* (b, 4H13[18]). In both complexes, the Q_p site is defined by TM helices 'C' and 'G' (shown as ribbons); additionally, in both complexes the site is occupied by quinone analogue inhibitors (stigmatellin in cytbc_1 and tridecylstigmatellin in cytb_6f). **c-d,** the arrangement of TM helices (shown as cylinders) within complexes shown in panels a-b viewed perpendicular to the membrane plane from the n-side of the membrane (extrinsic domains, loops and additional non-conserved subunits in the bc_1 complexes are not shown for clarity). **e-f,** A protein-free view of panels a and b showing the position of each quinone analogue in relation to catalytically essential residues and cofactors (shown as sticks). **g,** the PQ molecule resolved adjacent to the Q_p site in the spinach cytb_6f (6RQF[23]) in the context of its surrounding protein environment. The entrance to the Q_p site is outlined by a dark green dotted area shaded in light green. **h,** the two conformations of the Chl *a* tail, resolved in the spinach cytb_6f structure (6RQF[23]), control access to and from the Q_p site; an arrow is shown to indicate the direction of movement. A video of the conformational change undergone by the Chl phytyl tail depicted in panel h is provided in the supplementary material online. Subunits and prosthetic groups are coloured as in Fig 2, plastoquinone is coloured in yellow and is labelled 'PQ1', quinone analogue inhibitors are shown in purple and are labelled 'STG' and 'TDS' respectively.

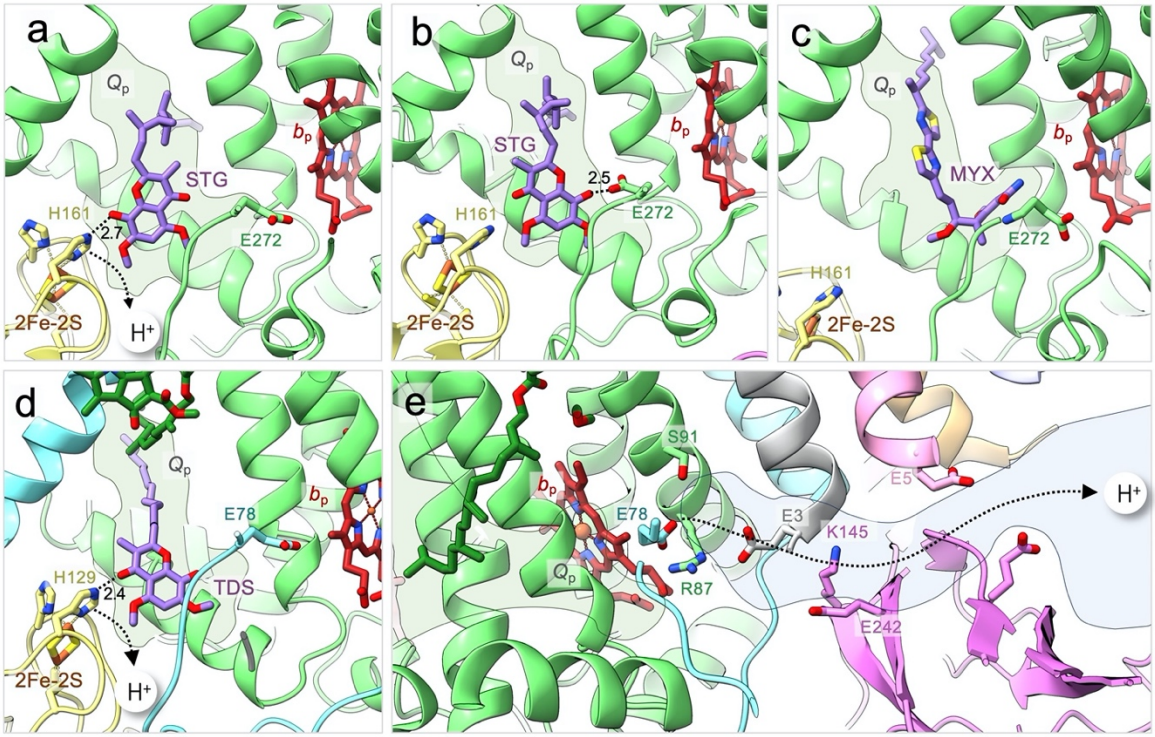

Fig. 6 | Proton movements during quinol oxidation at the Q_p site in cytbc_1 and cytb_6f. a-c, The binding of UQH_2 in the Q_p site of *G. gallus* cytbc_1 probed using quinone analogue inhibitors stigmatellin (**a,** 3BCC; **b,** 2BCC[33]) and bovine cytbc_1 with myxothiazol (**c,** 1SQP). **d,** Binding of PQH_2 within the Q_p site of *M. laminosus* cytb_6f probed using tridecylstigmatellin (4H13[18]). **e,** The putative exit pathway for the second proton from the Q_p site of spinach cytb_6f (6RQF[23]). An outline of the Q_p site is indicated by semi-transparent green shading while the putative proton channel is highlighted with semi-transparent blue shading. Putative proton exit pathways are indicated by black dotted lines and arrows. H-bond distances are indicated in (Å). Prosthetic groups, key catalytic residues and quinone analogue inhibitors are shown in stick representation with proteins shown as ribbons. Subunits, inhibitors and prosthetic groups are coloured as in Fig 2.

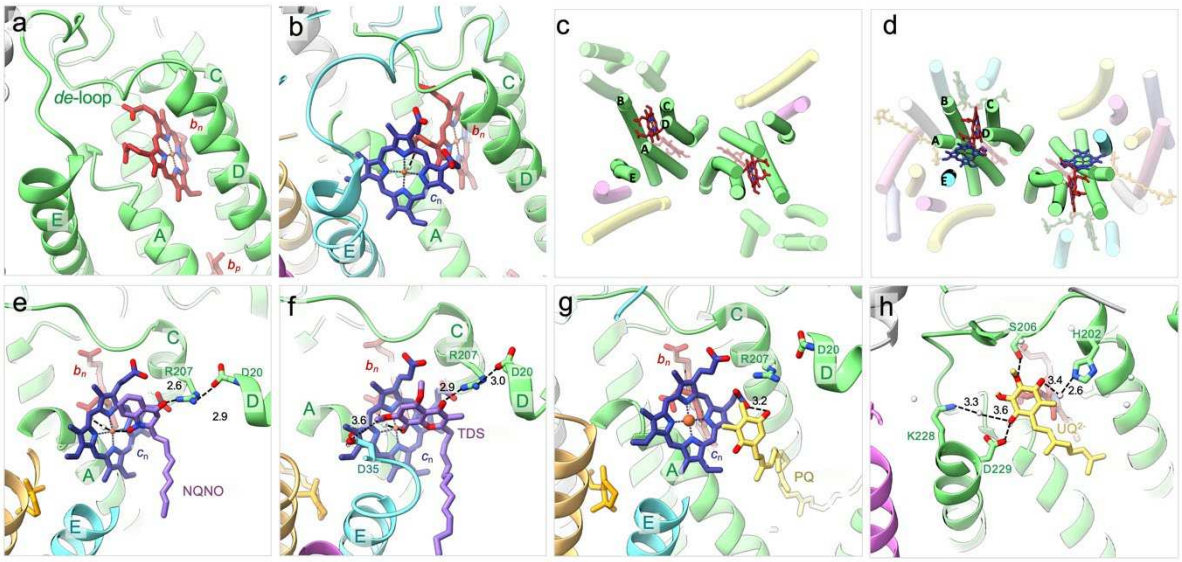

Fig. 7 | The Q_n sites of cytbc_1 and cytb_6f. a-b, a ribbon representation of the unoccupied Q_n site in the *G. gallus* cytbc_1 complex (a, 2BCC[33]) and the *Nostoc* PCC 7120 cytb_6f complex (b, 4OGQ[22]). In both complexes, the position of haem b_n between TM helices 'B', 'C' and 'D' is conserved, however in the cytb_6f (b) the additional c'-type haem (c_n) is present, this is connected to haem b_n via an intervening water molecule and obstructs access to haem b_n. **c-d**, the arrangement of TM helices (shown as cylinders) within complexes shown in panels a-b viewed perpendicular to the membrane plane from the n-side of the membrane (extrinsic domains, loops and additional non-conserved subunits in the cytbc_1 complex are not shown for clarity). **e-h**, ribbon representation of the occupied Q_n site in: e, the cytb_6f complex occupied by NQNO (e, 4H0L[18]); **f**, the cytb_6f complex occupied by TDS (f, 4H13[18]); **g**, the cytb_6f complex occupied by PQ (g, 6RQF[23]); and **h**, the cytbc_1 complex occupied with UQ (h, 1NTZ[66]). Prosthetic groups, key interacting residues and quinone analogue inhibitors are shown in stick representation with protein shown as ribbons. Distances between residues are shown by black dashed lines with distances indicated in (Å). Subunits, inhibitors and prosthetic groups are coloured as in Fig 2. Key water molecules are shown as white spheres.

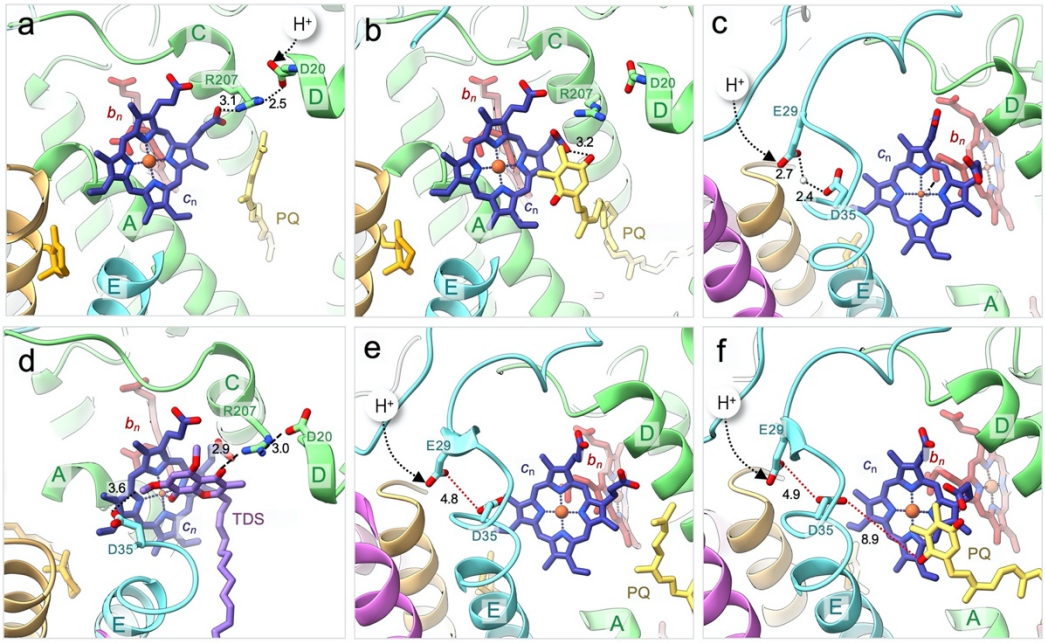

Fig. 8 | Conformational changes in the Q_n site of the cytb_6f complex may promote catalysis. a-b, a ribbon representation of the unoccupied **(a)** and occupied **(b)** Q_n sites in opposing halves of the spinach cytb_6f complex (6RQF[23]) showing conformational changes in the surrounding protein environment which may promote catalysis and allow proton uptake to the Q_n site via the putative D/R pathway**.** A video of the conformational changes depicted in panels a and b is provided in the supplementary material online. **c-d,** a ribbon representation of the unoccupied (**c,** 4H44[30]) and occupied (**d,** 4H13[18]) Q_n sites in *Nostoc* and *M. laminosus* showing putative components and conformational changes of the E/D pathway. **e-f,** a ribbon representation of the unoccupied (e) and occupied (f) Q_n sites in opposing halves of the spinach cytb_6f complex (6RQF[23]). Distances that are too far to facilitate proton transfer without the aid of intermediate water molecules are indicated by red dotted lines with the distances indicated below in (Å). Prosthetic groups, key catalytic residues, substrate and quinone analogue inhibitors are shown in stick representation with protein shown as ribbons. Key water molecules are shown as white spheres. Putative proton entry pathways are indicated by black dotted lines and arrows with H-bond distances indicated below in (Å). Subunits, inhibitors and prosthetic groups are coloured as in Fig 2.

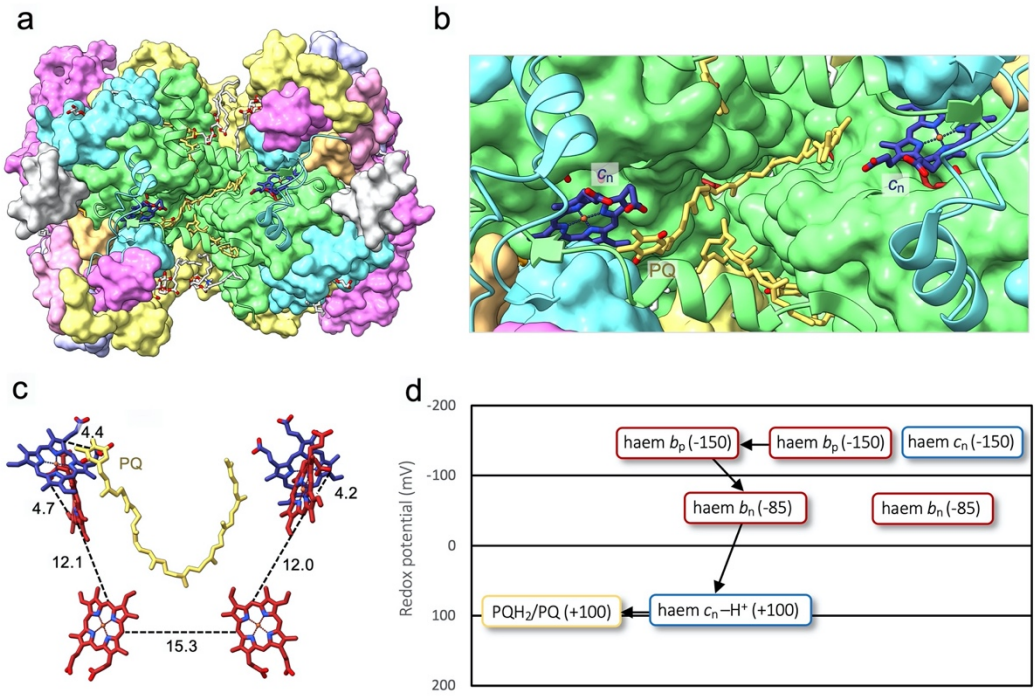

Fig. 9 | An electronic bus-bar lies within the core of the cytb_6f complex allowing electrons to move both within and between monomers via a bridge formed between the two haem b_p molecules. a, A stromal side view of spinach cytb_6f (6RQF[23]) showing the intermonomer cavity. Peripheral helices of cytb_6 and subIV are shown in cartoon representation for clarity. **b**, A zoomed-in view of the intermonomer cavity showing a PQ molecule (PQ2) traversing the two monomeric halves of the dimer between the two opposing haem c_n molecules. **c**, Edge-to-edge distances between the components of the low-potential electron transfer pathway in the dimeric cytb_6f. Distances are indicated by the black dashed lines with distances shown in Å. **d**, the redox-active components of the low potential pathway of cytb_6f shown on a scale of redox potential. The diagram shows the electronic connection between the two haem b_p molecules, which is facilitated by the short distance between the molecules (as shown in panel c). The midpoint potentials of the two c_n haems are proposed to be different, with the protonated c_n that binds PQ having a more positive potential than that of the c_n at the empty Q_n site [40,59]. Prosthetic groups and PQ molecules are shown in stick representation with protein in surface representation unless otherwise specified. Subunits, prosthetic groups and PQ molecules are coloured as in Fig 2.

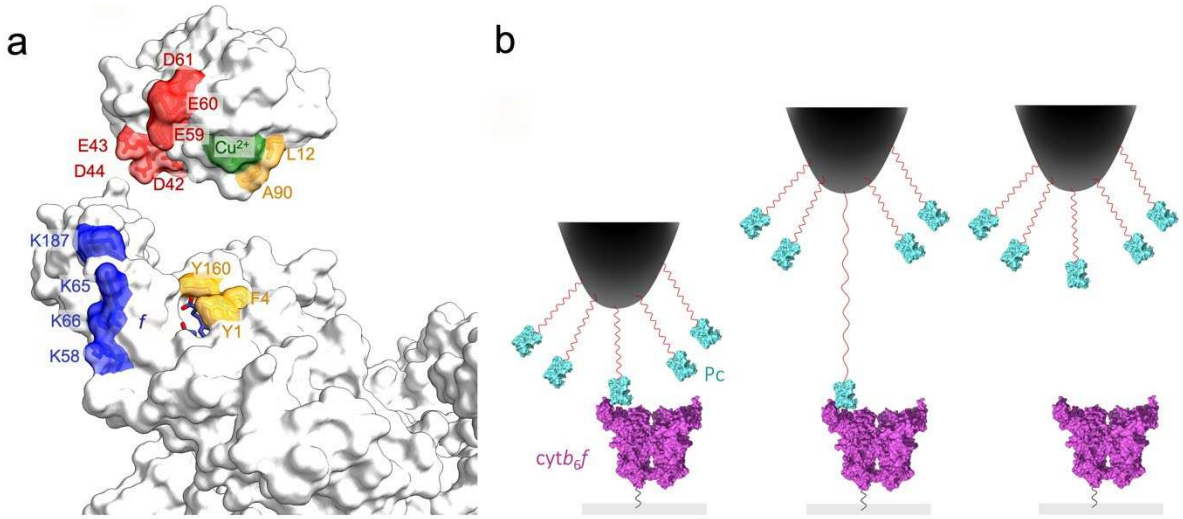

Fig. 10 | Interactions between cytb_6f and Pc. a, A surface view of cyt*f* (6RQF[23]) and Pc (1AG6[207]) showing the putative binding interface between the two complexes. Acidic residues are highlighted in red while basic and hydrophobic residues are highlighted in blue and orange respectively. Haem *f* is coloured deep blue as in Fig 2 while the Cu^{2+} centre of Pc and its coordinating residues are coloured green. **b,** A schematic showing the principle behind single-molecule force spectroscopy in characterising the interaction between cytb_6f and Pc. Cytb_6f (magenta) is depicted immobilised to a silicone oxide surface (shown in grey) while Pc (cyan) is attached to the AFM probe via a flexible 10 nm-long $SM(PEG)_{24}$ linker (red lines). The three panels shown depict the various stages of the experiment. In the first panel, one of the Pc proteins attached to the AFM probe binds to an immobilised cytb_6f; in the second panel the flexible linker is extended to its full 10 nm length as the AFM probe is withdrawn from the surface during the upward part of the tapping motion; in the third panel the force applied has exceeded the protein interaction force and has ruptured the Pc-cytb_6f interaction.

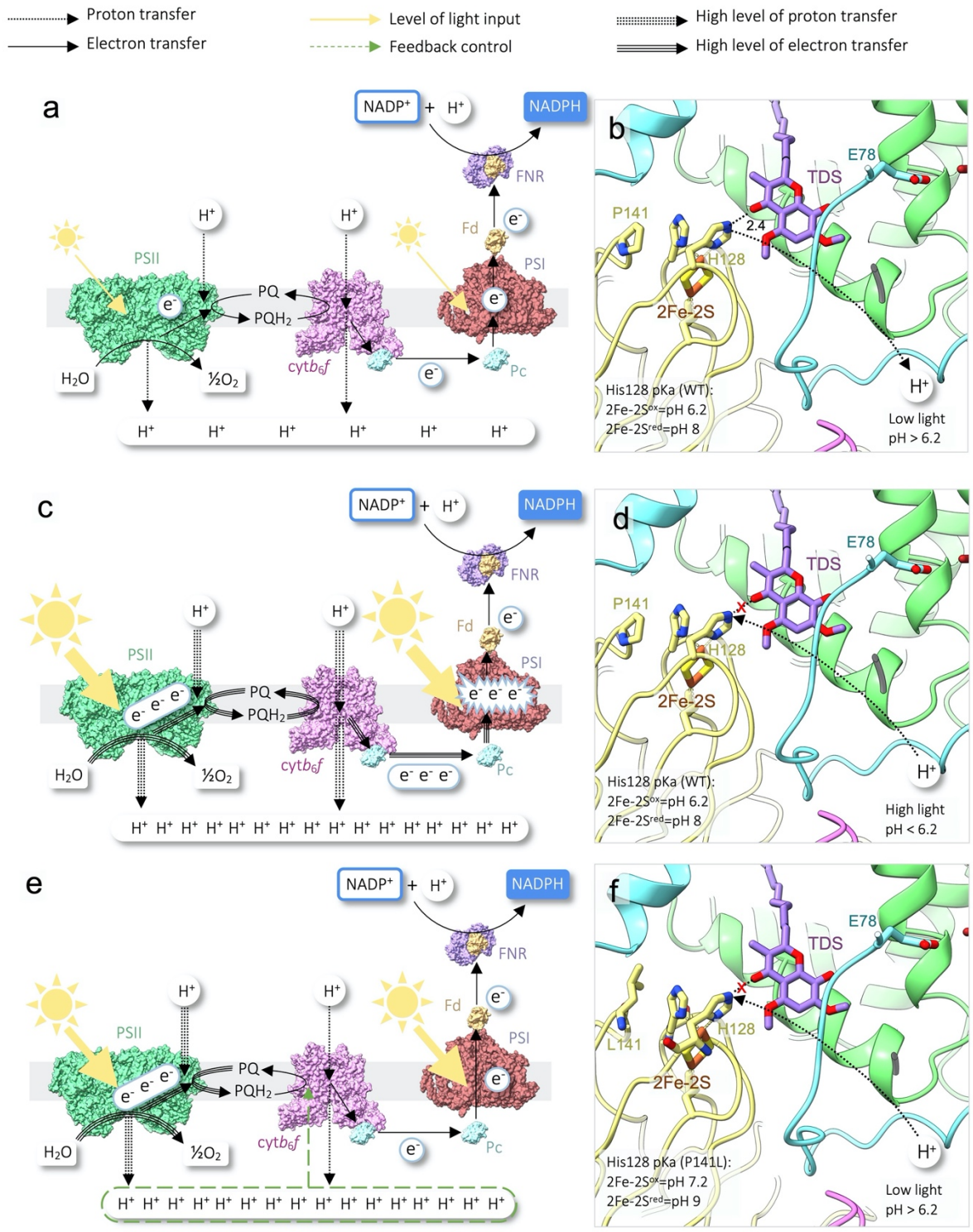

Fig. 11| Role of cytb_6f in photosynthetic control. In low light, LET rate is slow and proton deposition into the lumen remains low. The pKa of the His ligands of the 2Fe-2S ISP cluster is ~6.2 when oxidised and 8.0 when reduced, therefore, under these conditions where the lumenal pH remains above 6.2 the His ligands are unprotonated and therefore able to deprotonate PQH_2 (whose position inferred by binding of the inhibitor TDS) at the Q_p site facilitating cytb_6f turnover. **c,** In high light conditions, increased electron transfer through PSI exceeds the capacity of stromal/cytoplasmic electron acceptors resulting in acceptor-side limitation of PSI and photoinhibition due to damage associated with superoxide production.

d, In WT cells under high light, photoinhibition is mitigated by photosynthetic control. Here, the enhanced proton deposition into the lumen caused by an increased rate of LET results in a lowering of the lumenal pH to below 6.2. Lowered lumenal pH results in the protonation of the His ligands of the 2Fe-2S ISP cluster irrespective of whether it is oxidised or reduced. This disrupts PQH_2 oxidation at the Q_p site by inhibiting proton abstraction from PQH_2. **e,** In WT cells, the result of photosynthetic control is the slowing of PQH_2 oxidation at the Q_p site. This resultant oxidation of the high-potential chain (cyt*f*, Pc, P700) slows the rate of electron transfer to PSI. **f,** In the *Arabidopsis* P141L (ISP) mutant, the pKa of the His ligands of the 2Fe-2S ISP cluster is upshifted by 1 pH unit. This results in increased protonation of His and consequentially increased photosynthetic control (even under low light).

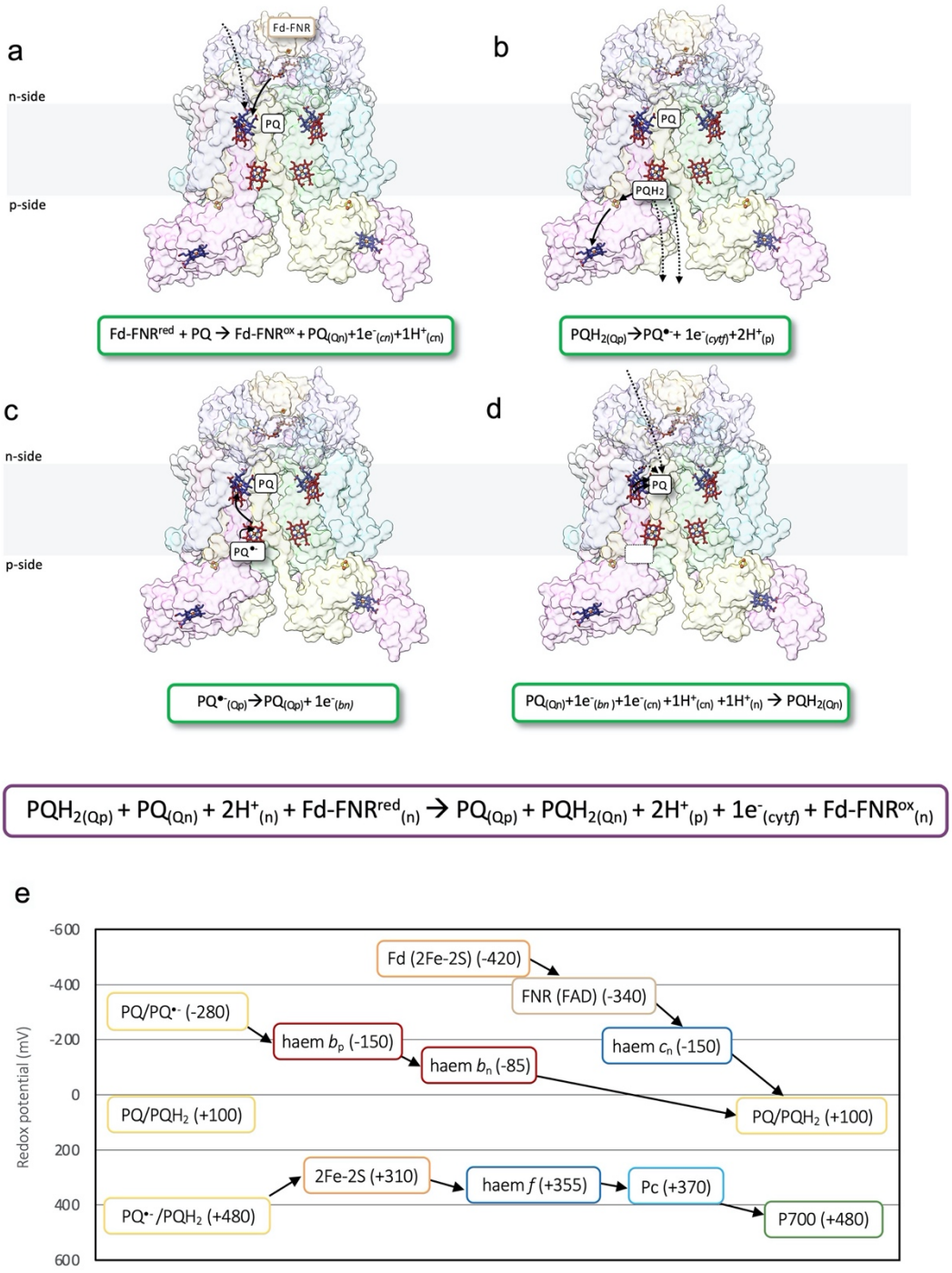

Fig. 12| Fd-assisted Q-cycle involved in cyclic electron transfer pathway 1 (CET1). The alternative Fd-assisted Q-cycle in cytb_6f (6RQF[23]) is proposed to involve the following steps; **a**, haem c_n is reduced via a bound FNR-Fd complex (1GAQ[208]) [208], reduction of haem c_n is coupled to its protonation [40]. **b**, Subsequent PQH_2 oxidation at the Q_p site results in reduction of cyt *f*, with two protons released into the lumen. **c**, The $PQ^{\bullet-}$ radical then reduces haem b_p which in turn passes the electron to haem b_n **d**, Quasi-concerted two electron-two proton transfer from the b_n^{red}-c_n^{red} pair to PQ results in production of PQH_2 at the Q_n site. Each reaction step is summarised below in a green box. The complete reaction is outlined below in purple. The position of the lipid bilayer that separates the stromal (n-) and

lumenal (p-) sides of the membrane is indicated by a grey stripe. The Q_p and Q_n sites are denoted by a white box overlaid on the structure with a solid outline indicating the site is occupied by substrate while a black dashed outline indicates the site is empty. Black dotted arrows indicate proton transfers while solid black arrows indicate electron transfers. **e,** Redox potential diagram of the cofactors involved in the Fd assisted Q-cycle. The midpoint potential of haem c_n is proposed to be downshifted due to interaction of cytb_6f with FNR. Midpoint potentials shown are those defined for the higher plants [204,205]

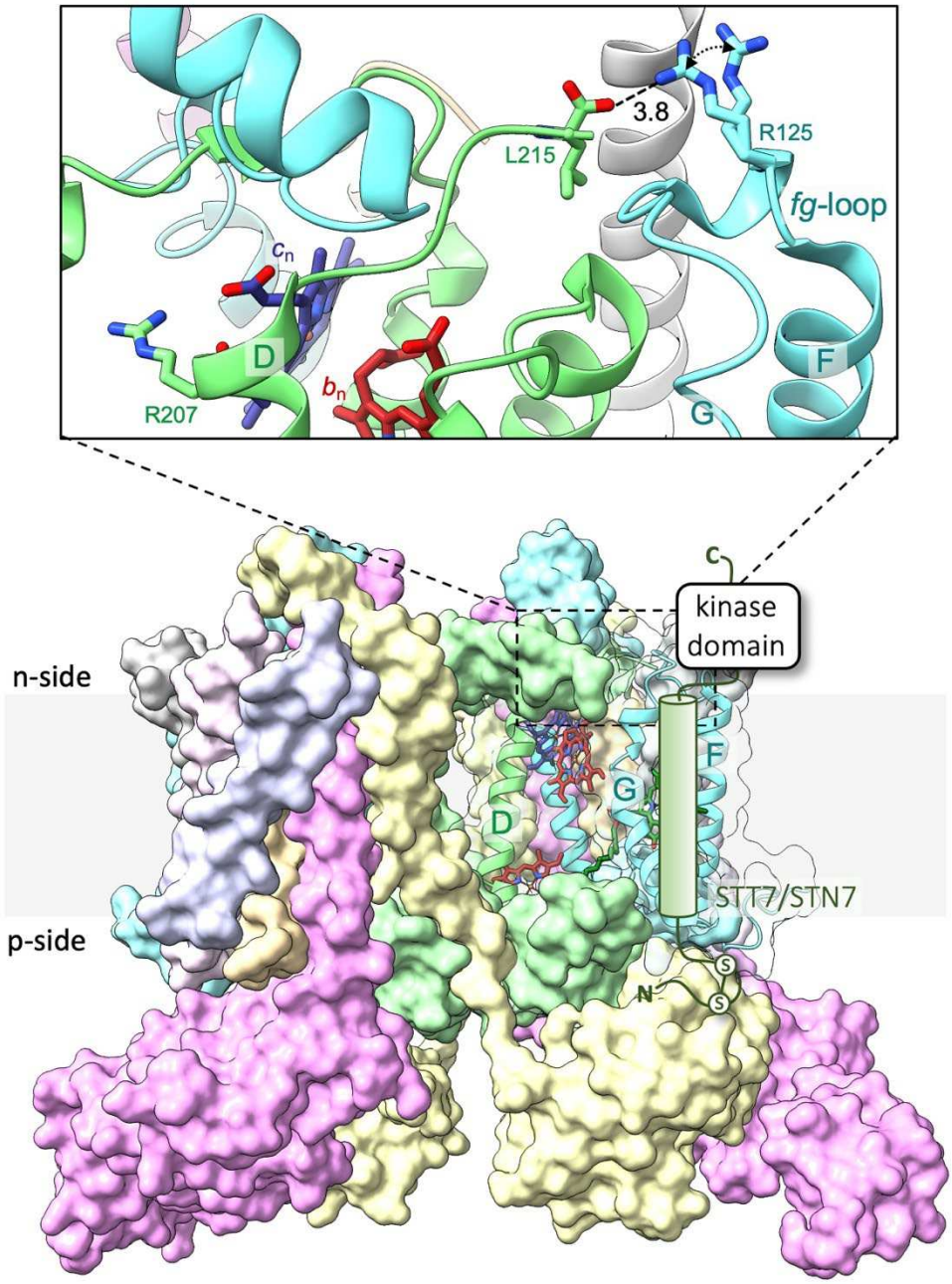

Fig. 13| Putative interactions between STT7/STN7 and cytb_6f. A schematic showing the proposed binding interface between STT7/STN7 and cytb_6f (6RQF[23]) involving the F and G helices (and the intervening *fg*-loop) of subIV as well as the ISP. A simplified drawing of STT7/STN7 is shown displaying the C-terminal kinase domain, TM helix (green cylinder) and short N-terminus containing two catalytically essential cysteine residues (Cys28 and Cys73). The two cysteine residues are shown forming a disulphide bridge which may be involved in kinase activation [196,199]. The zoomed-in panel shows stromal regions of subIV and cytb_6 shown in ribbon representation. This panel highlights a structural link

between Arg125 (subIV) and the Q_n site of cytb_6f via Leu215 at the C-terminus of cytb_6 and the Arg207 residue adjacent to haem c_n. Two conformations of Arg125 are observed in opposing halves of the dimeric spinach cytb_6f structure [23]. At the PQ bound Q_n site the Arg125 is rotated towards Leu215 and in the empty Q_n site the Arg125 is rotated towards the stroma. These two conformations may play a role in STN7/STT7 activity and release. Subunits and prosthetic groups are coloured as in Fig 2A.

Supplementary Video 1 | **Electron transfer via domain movement in the cyt*bc*$_1$ complex from *Gallus gallus*.** Two conformations of the Rieske ISP are observed in the *G. gallus* cyt*bc*$_1$, the Q_p proximal position and the Q_p distal position (1BCC, 3BCC[33]). Movement of the extrinsic portion of the ISP between these two positions facilitates electron transfer during ubiquinol oxidation. Prosthetic groups are shown in stick representation beneath a transparent protein surface while the ISP subunit is shown in the ribbon representation. Subunits and prosthetic groups within the complex are coloured as in Fig 2[33].

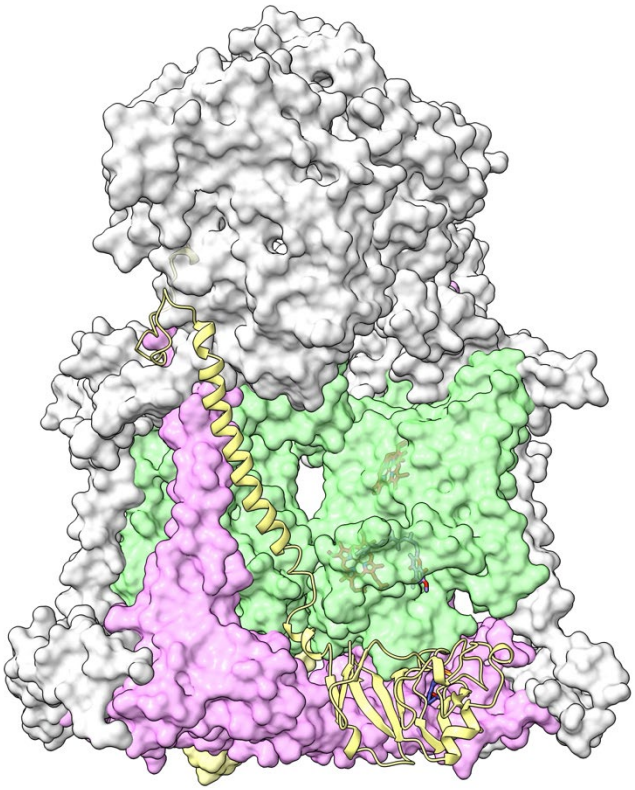

Supplementary Video 2 | **Conformational changes in the chlorophyll phytyl tail control access to and from the plastoquinol oxidation (Q_p) site in cytb_6f.** The two conformations of the chlorophyll tail resolved in the cytb_6f structure from spinach (6RQF[23]) control access of substrate to and from the Q_p pocket. Subunits are coloured as in Fig 2 [23].

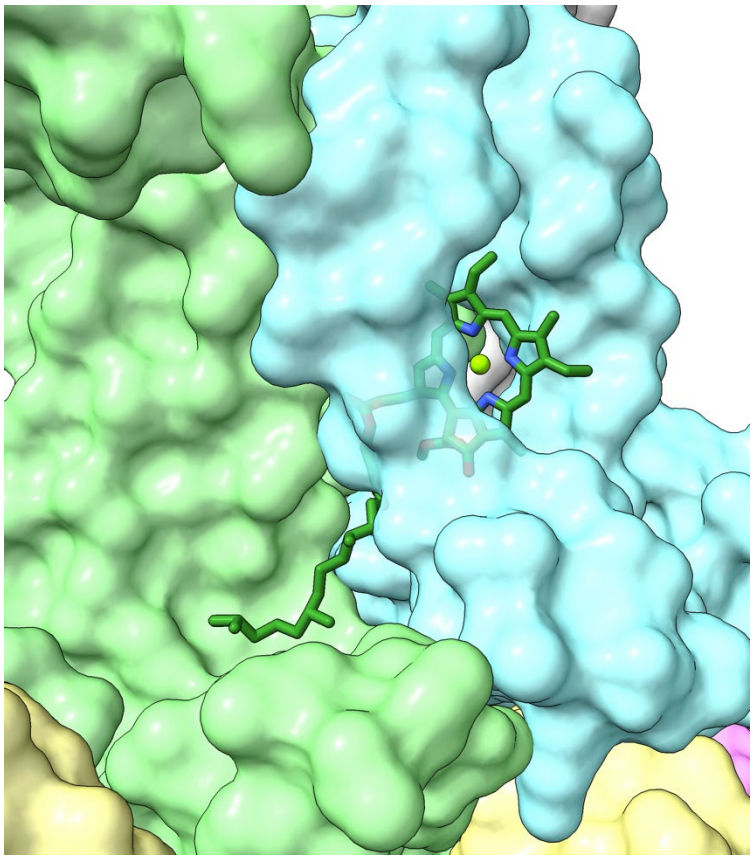

Supplementary Video 3 | **Conformational changes at the Q_n site of the cytb_6f complex may underlie catalysis.** Structural superimposition of the two halves of the spinach cytb_6f complex (PQ occupied Q_n site and unoccupied Q_n site) reveals conformational changes in the haem c_n propionates and nearby residues (R207, D20) which may underlie catalysis [23].